Heavy mineral analysis of Ice Complex sediments on Muostakh Island (NE Siberia)

Universität Potsdam

Erstbetreuer: Hanno Meyer
Zweitbetreuer: Bernhard Diekmann

Christoph Manthey
Matrikelnummer: 760797

09.03.2015

Abstract

This Bachelor's thesis focuses on the heavy mineral analysis of sediment samples taken in 2012 by an expedition team lead by Hanno Meyer from the Ice Complex formation on Muostakh Island in the Laptev Sea (NE Siberia). The heavy mineral analysis was used to investigate the provenance and transportation and sedimentation processes of the settled material. As influencing effects on the heavy mineral composition the origin of the material, further transportation energy and chemical weathering could be identified, which was also confirmed by a principal component analysis in combination with grain-size distribution data, provided by Hanno Meyer. The heavy mineral composition is dominated by amphibole, followed by pyroxene, garnet and opaque minerals. The origin indicating mineral leucoxene, appearing regional augmented, could not be identified. As provenance the Lena river could be identified by the use of comparative heavy mineral data. The sedimentation occurred in three phases. Between the first and second phase a hiatus in the stratigraphic record exist. ^{14}C-dating (Meyer (unpublished)) confirm this indicating a gap between ca. 41.6 kyr BP and ca. 19.7 kyr BP. This disconformity is caused by an erosional event. After this event chemical weathering took place at the top of the deposited layers of the first phase producing significant red aggregates. The second phase is characterized by higher transportation energy compared to the first and third phase, which is reflected by the appearing of rutile almost just in the corresponding unit and a more coarse grain-size distribution.

Zusammenfassung

Die vorliegende Bachelorarbeit beschäftigt sich mit der Schwermineralanalyse von Sedimentproben, welche während einer Expedition 2012 von ein Team, angeleitet durch Hanno Meyer, der Ice Complex-Formation auf der Insel Muostakh in der Laptev See (NO Sibirien) genommen wurden. Die Schwermineralanalyse wurde genutzt um die Herkunft sowie die Transport- und Ablagerungsprozesse des Materials zu untersuchen. Als beeinflussende Prozesse der Schwermineralzusammensetzung konnten die Herkunft des Materials sowie Transportenergie und chemische Verwitterung identifiziert werden, was zusätzlich durch eine Hauptkomponentenanalyse unter Zuhilfnahme einer Korngrößenanalyse, welche von Hanno Meyer bereit gestellt wurde, bestätig wurde. Die Schwermineralzusammensetzung ist dominiert von Amphibol, gefolgt von Pyroxen, Granat und opaken Mineralen. Das Mineral Leukoxen, welches herkunftsindikativ ist und regional gehäuft auftritt, konnte nicht identifiziert werden. Der Fluss Lena konnte mithilfe vergleichender Schwermineraldaten als Herkunft bestimmt werden. Die Sedimentation fand in drei Phasen statt. Zwischen der ersten und zweiten Phase exisitiert eine Schichtlücke in der stratigraphischen Abfolge. ^{14}C-Datierungen (Meyer (unveröffentlicht)) bestätigen dies durch eine Unterbrechung zwischen ca. 41.6 kyr BP und ca. 19.7 kyr BP. Diese Diskordanz ist durch einen erosiven Prozess entstanden. Nach diesem Prozess setzte chemische Verwitterung an den oberen Schichten des abgelagerten Materials der ersten Phase ein. Die zweite Phase ist im Vergleich zur ersten und dritten Phase durch höhere Transportenergie charakterisiert, was durch das Auftreten von Rutil in fast nur dieser Einheit wiedergegeben wird.

Eidesstattliche Erklärung

Hiermit erkläre ich, dass ich die vorliegende Bachelorarbeit mit dem Thema

"Heavy mineral analysis of Ice Complex sediments on Muostakh Island (NE Siberia)"

vollkommen eigenständig verfasst und nur die angegebenen Quellen und Hilfsmittel verwendet habe. Alle Stellen, die dem Wortlaut und dem Sinne nach von anderen Arbeiten stammen, habe ich durch Angabe der Quelle als Zitat kenntlich gemacht. Diese Arbeit wurde in gleicher oder ähnlicher Form weder einer anderen Prüfungsbehörde vorgelegt noch veröffentlicht.

Christoph Manthey

Acknowledgements

I want to thank Hanno Meyer and Bernhard Diekmann from the Alfred-Wegener-Institute for giving me this opportunity to work on this current research topic and supporting me over the complete distance of the analysis and writing process.
But overall I want to give a big thank you to my family for always having my back straight up and to Till, Marty and Marc carrying in the harder times for my physical and mentally welfare.

Contents

List of Figures

List of Tables

Abbreviations

Abbreviation	Meaning
%	percentage
°C	degree Celsius
cal. ka BP	calibrated thousands years before present (1950)
cm/yr	centimeters per year
g/cm^3	gram per cubic centimeter
LGM	last glacial maximum
m asl	meter above sea level
m/yr	meter per year
PCA	principal component analysis
SPT	sodium polytungstate
yr BP	years before present (1950)

1 Introduction

Climate change is one of the nowadays biggest topics in the society, politics and science. Its complexity is still not completely understood and its impact will need new ground-breaking solution in a multidisciplinary way on different levels of economy, politics and science. In this purpose it is required to understand the development and effect of earth processes in the past. This enables understanding of present process and a scientifically backed reaction on them. This concept is formally known as uniformitarianism founded by James Hutton in 1975.

The Arctic with its periglacial environments is an area of big interest. One of its main features is the permafrost, which underlays a huge amount of the earth' surface (25%, French 1996). These permafrost regions response very sensitive to climatic change (Meyer *et al.* 2015a), which can have different impact on people living in this areas and world wide. Hence, the understanding of geological processes is a fundamental requirement.

Muostakh Island lies in the area of periglacial environment and is mainly build up of Ice Complex sequences. These Ice Complexes are good archives for reconstruction of Quaternary paleoclimatic conditions, as recently shown in Meyer *et al.* (2015b), because of its ability to preserve information via macro- and micro fossils, stable isotope records and sedimentation processes. Because of recently ongoing thermo-erosion and thermo-denudation processes in the summertime the area of the island shrinks continuously. This makes it an area of high interest, because of its limited availability for researches.

The provenance analysis is based on heavy mineral analysis and meant to be a tool to reconstruct the geological development of the island with the origin and transportation processes of the settled material. With its help the paleoenvironmental history of Muostakh Island and the adjacent areas can be lifted a bit more and understood way better.

2 Scientific Background

2.1 Periglacial Environment

The term of "periglacial" areas was introduced by von Lozinski in 1909 and describes the areas at the edges of the Pleistocene ice sheets and glaciers (French 1996). Nowadays there exist a few variable definitions for the periglacial area depending on the field of studies. According to French (1996) periglacial environments are non-glaciated areas dominated by frost-action and permafrost-related processes. The climatic conditions for these are defined as regions with an annual mean temperature lower than +4°C (Williams 1961), what was later redefined to +3°C and sub-divided in frost-action dominated (-2°C) and frost-action attended (-2 to +3°C) regions (French 1996). The periglacial environment in the northern hemisphere can be sub-divided in the Alpine periglacial zone, the Subarctic-maritime periglacial zone, the Subarctic-continental periglacial zone, the Boreal periglacial zone, the Tundra zone, the Arctic frost-debris zone and the High Arctic frost-debris zone (Karte 1979, Figure 2.1).

Permafrost is a part of periglacial environments and describes a layer of frozen ground, which does not completely thaw in the summer (French 1996) for at least two years (Higgins & Coates 1990). The regions in which it appears can be subdivided by the percentage area underlying by permafrost as continuous (90 to 100%), discontinuous (50 to 90%), sporadic permafrost regions (10 to 50%) and areas with isolated patches (0 to 10%, Zhang *et al.* 1999) and furthermore regional as polar, subsea, plateau and alpine permafrost regions (French 1996).

The ground in the Permafrost regions is cryologically subdivided in the active layer (Supra-permafrost layer), the Permafrost layer, the unfrozen ground beneath the Permafrost layer (Sub-permafrost talik) and unfrozen zones inside the Permafrost layer, termed talik (see Figure 2.2, French 1996).

The processes described by the term frost-action are generally based on alternate freezing and thawing in soil, rock and sediments (French 1996). Mainly they are ice segregation, which is connected to frost heave, and the development of frost

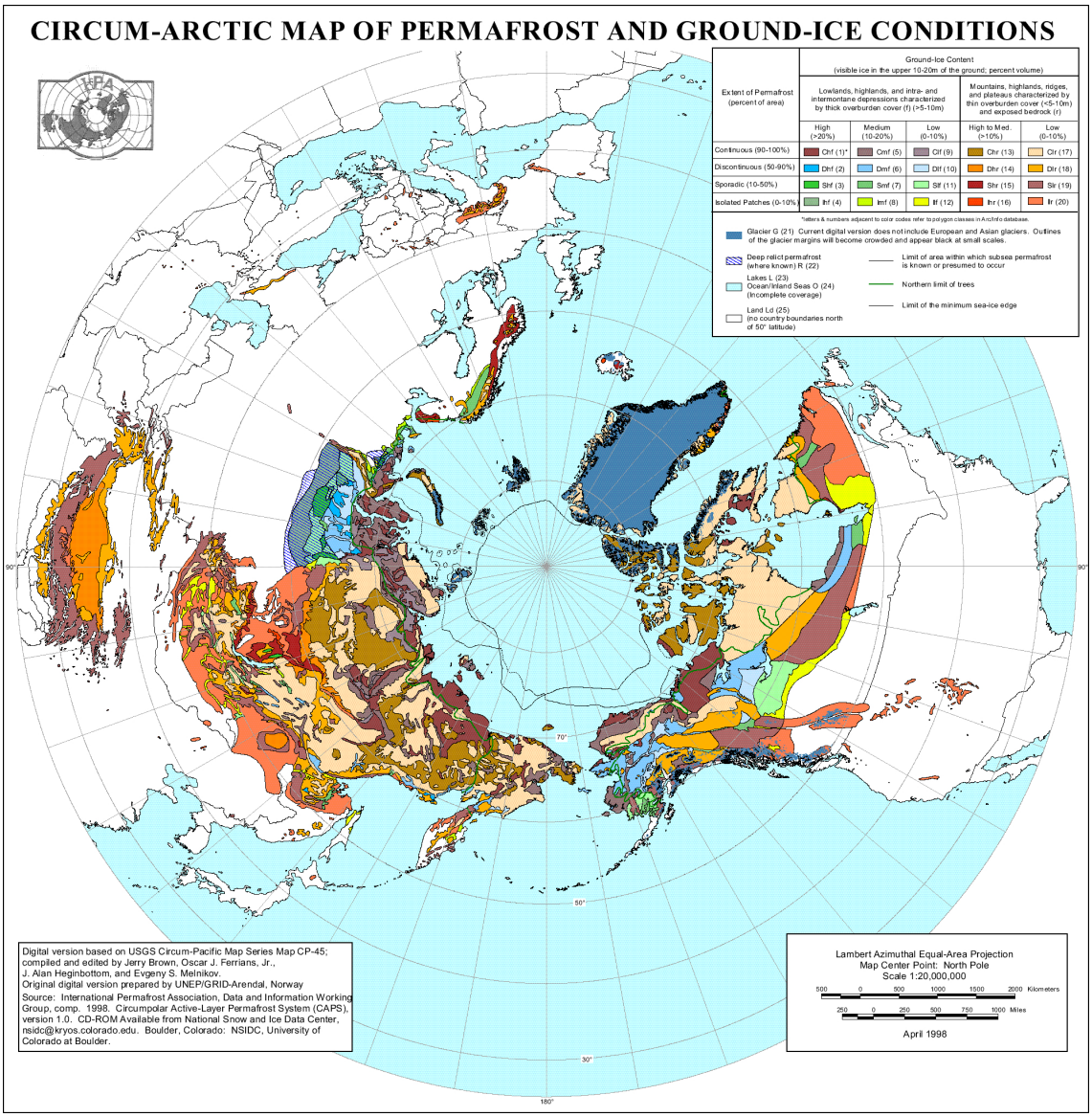

Figure 2.1: Circum-Arctic Map of Permafrost and Ground-Ice Conditions by Brown *et al.* 1998 for International Permafrost Association

cracks, which gives the impulse for cryogenic weathering and further leads to the building of ice, sand and soil wedges. Obviously the properties of these processes are based on the characteristics of water in freezing and thawing processes and its interaction with solid material and grains in the ground. The term ice segregation describes the formation of ice lenses through capillary action in the ground. In case of forming ground ice, water, which is located beneath this layer, penetrates upward to it by capillarity. This works as long as the pressure of the water (P_w) beneath the ice is higher than the pressure of the ice (P_I) itself. When the P_w exceeds P_I the ice lense and the overlaying sediment will be heaved upward, what is called "frost heave". Frost cracking is a process induced by increasing and decreasing temperatures in ice-frozen soils. The resulting vertical cracks fulfilled with

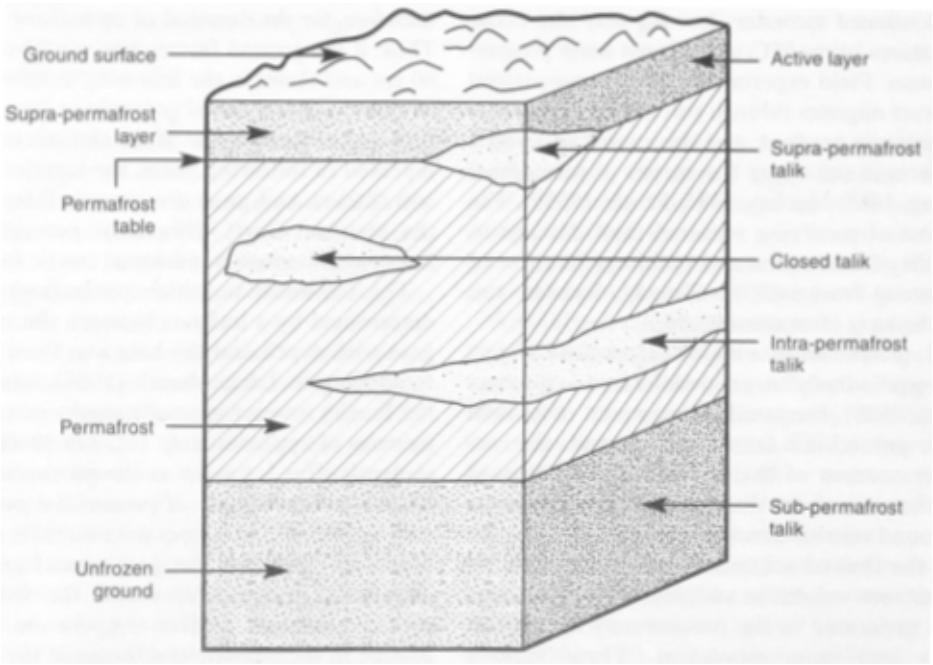

Figure 2.2: Examplary crosssection of Permafrost (French 1996)

material form cryogenic structures, which are named ice wedges, sand wedges or soil wedges, depending on the fulfilling material (French 1996). Ice wedges have to be mentioned, because of their significant role in forming the characteristic periglacial morphological feature of polygon nets (French 1996) and their ability of containing paleoclimatical information in continental areas with less provided archives, espacially in Siberia (Meyer *et al.* 2002). Another important group of features is summarized by the term Thermokarst. It describes karstlike morphologies, which are not formed by the dissolution of material, but the melting of ground-ice and ice-rich permafrost for different reasons, and all effects connected to it (Higgins & Coates 1990). There are mainly four geomorphological structures described: Thermokarst pits, beaded streams, thermokarst mounds and thermokarst/thaw lakes (Higgins & Coates 1990). A geomorphological feature with a high scientific interest is the "Ice Complex". "Ice Complex" is a term for ice-rich, syngenetically frozen deposits of the late Pleistocene in the Arctic periglacial zone (Schirrmeister *et al.* 2013), which are also called "Yedoma". The formation process is still under discussion. Fluvial (i.e. Rozenbaum 1981), aeolian or cryogenic-aeolian (i.e. Tomirdiaro & Chernenky 1987), proluvial (i.e. Gravis 1969), polygenetic (i.e. Sher *et al.* 1987), the formation through meltwater of perennial snowfields (i.e. Galabala 1997) and further through ice-dams (Grosswald 1998) or deltaic environments (Nagaoka *et al.* 1995) are discussed (Schirrmeister *et al.* 2002). Schirrmeister et al. (2013) summarized Yedoma as "a characteristic periglacial facies whose formation is controlled by the interaction of several climatic, landscape, and geological preconditions typical for non-glaciated Arctic lowlands". They are used as paleoenvironmental and paleocli-

matic archives. The information are included as composition of stable isotopes in the ice wedges, fossils in the sediments and geochemical data (Grosse *et al.* 2007). Furthermore stratigraphical researches about the origin of the settled material are possible, which allow to draw a fuller picture of the development of the landscape. One of them is the heavy mineral analysis.

2.2 Provenance Analysis

Provenance analysis is a suitable method to investigate the origin of sediments and sedimentary rocks. It is based on the principles of sedimentology, whereupon a settled material is related to its source and its way of transportation. The use of heavy minerals as tracers is a reliable tool and was already successfully used in North Siberia for instance for sedimentological pattern of material influx into the Laptev Sea (i.e. Peregovich 1999, Behrends 1999). Generally heavy minerals are understood as siliclastic minerals with a density higher than 2.89 g/cm^3 (Boenigk 1983). Like all sedimentary material the enrichment and shape of heavy minerals is the result of the provenance and the time, length and energy of transportation. The fraction of heavy minerals itself is used preferredly in their ability to give a more specific signal of their origin than lighter minerals like quartz or feldspar (Mange & Maurer, H. F. W. 1992), because of their higher resistance against physical and chemical abrasion (Boenigk 1983). Even so it has been considered that the composition and material can be also modified while the transportation by physical sorting, mechanical abrasion and dissolution, what can change the original signal of the provenance and lead to erroneous conclusions (Morton & Hallsworth 1999). The main influences in here are the hydraulic conditions in the transportation and diagenesis after sedimentation, which leads to dissolution (Morton & Hallsworth 1994).

3 Study Area

3.1 Laptev Sea

The Laptev Sea is an epicontinental shelf sea, which lies in the Arctic Ocean, with a depth of 20 m in huge parts of it (475 000 km, 70%, Drachev *et al.* 1998) and belongs to the continental margin of northeastern Asian in the Arctic (Drachev *et al.* 1998), which is part of the tundra zone of the periglacial areas at the North Pole (Schirrmeister *et al.* 2013). The shape of this margin is mainly based on a Late Mesozoic folding and a Tertiary rifting, which began 56-58 Ma in consequence of the opening of the Eurasian Basin and can be summarized in four periods (see Table 3.1, Drachev *et al.* 1998). Thereby the Lena-Rift-System developed (Drachev *et al.* 1998). During the LGM the shelf area was exposed due to the lower sea level (Bauch *et al.* 2001) and degraded by five runways in North-South direction through a lower sea level (Holmes & Creager 1974). Approximately from 14.2 until 5 cal. ka BP the Arctic Ocean transgressed again to the present sea level and flooded the basin in four intervals (Bauch *et al.* 2001). During this transgression several sedimentation processes took place and settled sediments of terrestrial and marine origin on the shelf (Bauch *et al.* 1999). The resulting sea gains recently freshwater input and sediment flux by the rivers Khatanga, Lena, Anabar, Yana, Olenek, Omoloy and also sediment flux by the Kara Sea (Peregovich 1999, Müller & Stein 2000).

Table 3.1: Periods of the formation of the Laptev continental margin according to Drachev *et al.* 1998

Phase	Time	Tectonic Process
1	End of Paleocene and Eocene	extensive rifting
2	Oligocene to Middle Miocene	non-rift, compression and/or transpression regime, with very slow (less than 0.2 cm/yr) spreading
3	End of the Middle Miocene to Middle Pleistocene	resumption of the rifting
4	Middle Pleistocene to today	deceleration of spreading in the Eurasia Basin

The Muostakh Island is placed in the Buor Khaya Gulf of the Eastern Laptev Sea

on a shoulder of the Ust-Lena-Rift (Drachev *et al.* 1998). The closest and most important town in this region is Tiksi in case of climate information, logistic and industry.

3.2 Muostakh Island

The coordinates of Muostakh Island are 71° 34' 30" N, 130° 0' 40" E (Günther *et al.* 2013a). The island is composed of Ice Complex sedimentary sequences (Yedoma) from sea level up to 20 m asl (meter above sea level, Meyer *et al.* 2015b), and believed to be a Pleistocene "remnant[s] of an accumulation plain in front of the Kharaulakh Ridge". The Kharaulakh Ridge developed in the permo-carboniferous era (Schirrmeister *et al.* 2011). It is assumed that the island was once connected to the continent at the Bykovsky Peninsula and be part of a wider accumulation plain in the Laptev Sea region (Grigoriev 1993). The landscape of this area transformed during the early to middle Holocene warming to a thermo-karst dominated relief (Grosse *et al.* 2007). Recently one of the highest thermo-erosion rates about 10m/yr (meter per year) occurs at the coastline of Muostakh Island (Günther *et al.* 2013a, Günther *et al.* 2013b), because the area underlain by continuous permafrost is exposed to abrasion by wave energy in the summertime (Günther *et al.* 2013a) while the local temperature supports thawing of the ground ice.

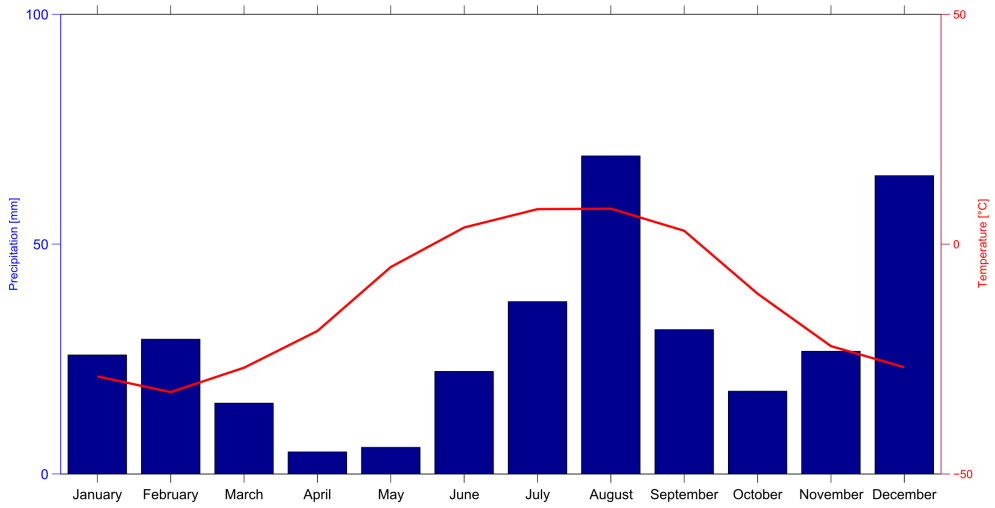

Figure 3.1: Mean monthly precipitation and temperature of Tiksi for the time from October 2003 till December 2007, data from Kloss (2008)

The Muostakh Island belongs like the town Tiksi to the Siberian Province of the Arctic Climate Zone (Shahgedanova 2002). The mean annual temperature for Tiksi

as the closest meteorological station is recorded with -12.8°C and the mean annual precipitation with 394.2 mm from October 2003 to December 2007 (Kloss 2008). The highest temperatures are reached in July and August, whereas the lowest are reached in January and February. August and December are the months with the highest amount of precipitation, whereas the smallest amount of precipitation is in April and March. This leads mainly to physical weathering processes. Figure 3.1 shows the climate situation more in detail, based on the data of Anna Kloss.

The geological and cryolithological features are described by Meyer *et al.* (2015) and drawn schematically in Figure 3.2. The Yedoma formation can be subdivided into three units. The lowest unit is approximately 8 m thick and consists of mostly sandy silt layers with a high content of ground ice alternating with thin peat layers, which are finally limited to the top by an 1 m thick peat layer. This layer exists in all outcrops on the island. In this unit ice wedges developed with a width of ca. 4-5 m. The age of this layer is dated with between ca. 45860 yr and 41625 yr BP (Meyer, unpublished).

The overlying unit is approximately 9 m thick and borders discordantly the first unit, as indicated by an erosional plane and the dated age of ca. 19760 yr BP at the bottom and ca. 16107 yr BP at the top (Meyer, unpublished). The layers consists of coarser sand to gravelly material with lower ground ice content and lower organic content compared to the first unit. The ice wedges in this sub-formation have a width of ca. 1-3 m.

The sediment of the middle unit indicates a higher energy of transportation than in the lower one, which is supported by an erosional plane between the lower and middle units. Another indication is given by the shape of the ice wedges. Since the material was deposited faster and the ice wedge had less time to build up, which led to their thinner width.

The highest and youngest unit reaches a thickness of about 4-5 m and is not continuous. It is build up by about ca. 10 m wide patches of organic-rich and ice-rich sandy silts and cut by ice wedges with a width of generally less than 1 m, but also 3-5 m, what can reach downward into older layers (Meyer *et al.* 2015b).

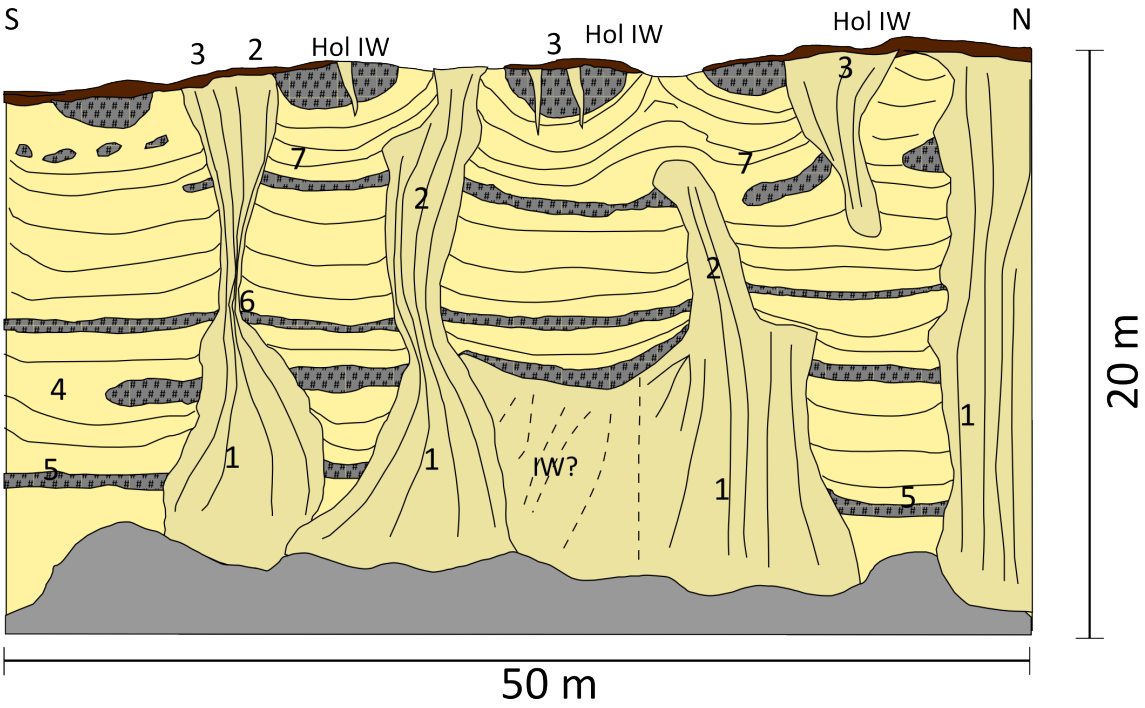

Figure 3.2: Schematic keysection Muostakh Island, compiled after a fieldbook drawing of Hanno Meyer, (1) Pleistocene ice wedges (first generation) 3-5 m width, (2) Pleistocene ice wedges (second generation) 1-3 m width, (3) Holocene ice wedges, variable in width, (4) prominent peat layer, up to 1 m thick, ca. 8 m asl, (5) to (7) peat layers, 0.5m thick

Figure 3.3: Foto of the compiled keysection in Figure 3.2, view from the northeast to the southwest, foto by Hanno Meyer

4 Methods

4.1 Sampling

The analyzed samples were taken from outcrops on the eastern side of the Muostakh Island (Figure 4.1) in 2012 by an expedition team lead Hanno Meyer. They cover a range from 4 to 20 m asl within three outcrops with nearly horizontal layers. Thus they include the whole sedimentary sequence of the island. Profile 1 and 2 were sampled from the bottom to the top, while profile 3 was sampled from the top to the bottom. Table 4.1 shows the belonging of the each sample to the stratigraphic units. The samples were transported in the frozen state to the Alfred-Wegener-Institut (AWI) in Potsdam, where they were thawed and dried under controlled conditions.

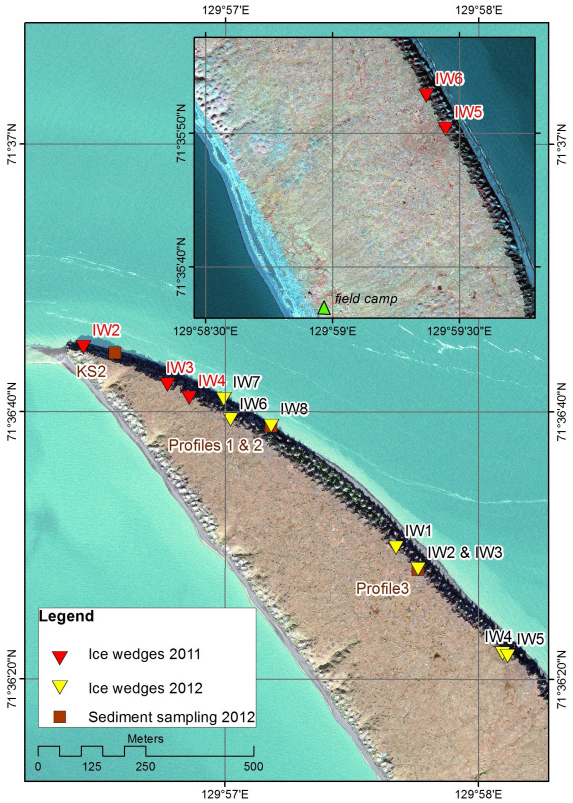

Figure 4.1: Map of Northern part of Muostakh Island, outcrops marked with red squares (profile 1, 2 & 3)

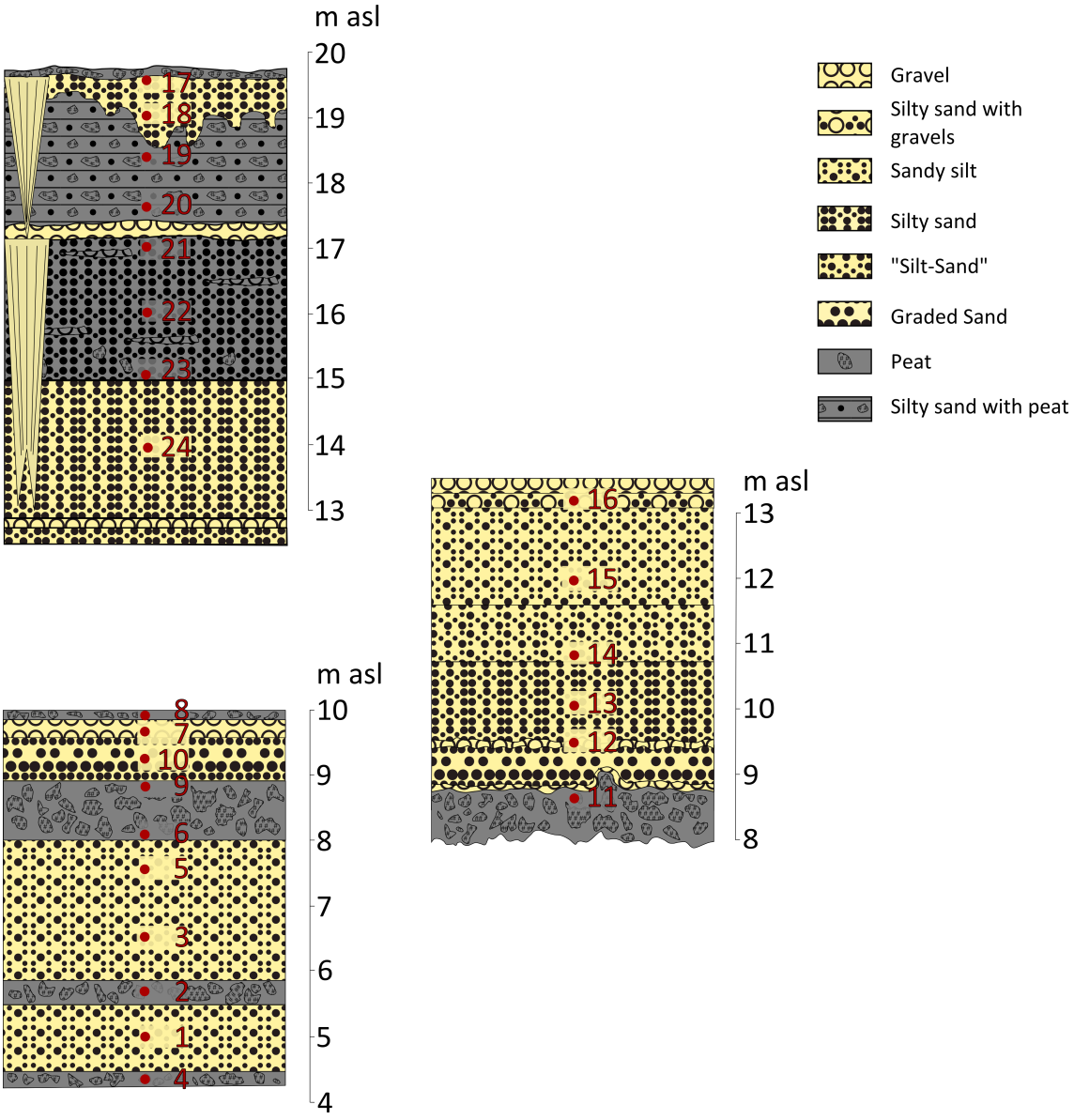

Figure 4.2: Schematic drawing of the sampled outcrops with relative position of the samples MUO12-SS-01 to MUO12-SS-24

Table 4.1: Correlation of samples to stratigraphic units

Unit 1	Unit 2	Unit 3
MUO12-SS-01 to -06, MUO12-SS-09/-11	MUO12-SS-07/-08 MUO-SS-10 MUO12-SS-12 to -16 MUO12-SS-21 to -24	MUO12-SS-17 to -20

4.2 Processing

Provenance analysis has been carried out under a microscope by counting heavy mineral grains. For this purpose, it is necessary to extract them from the fraction between 63 and 125 μm of the sediment samples by sieving and density slicing. This fraction is recommended by Morton and Hallsworth for the determination of provenance-sensitive heavy mineral ratios (Morton & Hallsworth 1994). Afterward slides for the microscope were made.
Sieving is a method to separate sediments in accordance to their grain size. Therefor the sediment is moved in any direction by vibration and/or shaking until the particles which are smaller than the mesh size are separated from the bigger ones. Grain size is classified by the Wentworth-Scale, a widely used numerical scale, which divides the particles by the negative logarithm of the diameter to two (Tucker 1996). The numerical description is the phi-scale with D for the diameter of a grain.

$$\phi = -log_2 D$$

Wet sieving refers to sieving to a sample in a water-sediment-mixture. It is used to divide the samples in clay and silt-sand-fraction. Therefor the material has to be mixed with water first for one day in a horizontal shaker until the mixture is assumed to be homogenous. Then it is filled in a sieve with a mesh width of 63 μm and sieved for ten to 15 minutes in addition of pure water. The sieve is connected with a ultrasonic tool named Rhewum Schallfix which shakes the sieve with a frequency of 50Hz. The smaller size fraction is kept in the water-sediment-mixture which is necessary for further processing such as clay mineral analysis (i.e. Atterberg). The larger fraction is put in a dish into a drying oven for the dry sieving process. After drying the fraction bigger than 63 μm, the preparation of the samples continues with dry sieving. Therefor the sample is shook in a stack of two sieves with the mesh widths of 63 μm and 125 μm for eight minutes. This separates the samples in fractions of grain sizes smaller than 63 μm, between 63 μm and 125 μm and larger than 125 μm. For this purpose the ATM Sonic Sifter is used. The fraction smaller than 63 μm exist, because wet sieving is not fully separating the samples. Afterward the samples weighed and the fraction between 63 μm and 125 μm is used for the density slicing.
In the process of density slicing the minerals of the samples are separated by their density into two fractions, one more and one less dense than a defined threshold. In our case the threshold is 2.86 g/cm^3 to extract the heavy minerals. Therefor a solution of sodium polytungstate and pure water (SPT-solution) is prepared with the required threshold. 10 ml of the SPT-solution are added to each sample in a

separate centrifuge tube, shaken, sonicated, shaken again and then centrifuged with 3000 rotations per minute for 20 minutes. This separates the sample in a heavy and light fraction. Afterward the heavy fraction is shock-frosted in a N_2-bath, such as the light fraction of a sample can be separately filtered through a single filter for each. It is also washed with distilled water to clean it from SPT leftovers. Afterward this is repeated for the heavy fractions, so each fraction of the samples corresponds to a single filter. Subsequently the samples are put in a dry oven at 50°C for the next work step.
To finish the processing of the sample the last step is to prepare the compounds for the microscopic investigation. For this purpose a small heap of 2x2 mm^2 of each sample is spread on an object plat out of glass. Then a thin glass, 21x24 mm seized, to cover the compound was brushed with a heated synthetic thermal plastic named Meltmount 1.68 as mount, which has a specific optical refraction of 1.68, and put on the spread sample the plastic downside on the material. The temperature to melt the plastic to a good viscous material is 67.5°C. Then the slides are examined under a polarization microscope type.

4.3 Microscopy

Microscopy with polarized light is one of the fundamentals in geology to get more detailed information about rock samples (Stoiber & Morse 1994). The microscopes used in these studies were the ZEISS Axioskop type B microscope for analysis and .... for photos. The application for sedimentological studies with sprinkled material on slides like in this thesis works similar to the research with thin section of igneous and metamorphic rocks. Minerals are characterized by their shape, cleavage properties, color, fraction, relief, pleochroism, extinction, birefringence, elongation and interference figure (Boenigk 1983, Mange & Maurer, H. F. W. 1992). The shape, cleavage properties, color, fraction, relief and pleochroism are characterized with single polarized light. The color of a mineral is made by the process of absorbing light of specific wave lengths running through the grain (Stoiber & Morse 1994). Pleochroism is the effect that the absorbed wave lengths change while rotating the grain through the polarized light, so the color itself changes (Boenigk 1983, Stoiber & Morse 1994). Every grain has a black boundary at its edge to the mount. The thickness of this boundary depends on the difference between the optical refraction of the mount and the optical refraction of the mineral. The larger the difference is, the larger the boundary (Boenigk 1983).
Birefringence, extinction and elongation are studied with double polarized light. Birefringence is the phenomena which appears when the light wave entering the mineral is split into two perpendicularly polarized waves with different velocity. So,

these waves interfere characteristically (Boenigk 1983). The intensity of it depends on the relative position of the grain to the polar filters. This changes due to rotation of the grain from the maximum intensity to black, which is called extinction (Boenigk 1983). For the elongation an additional material with a birefringence is inserted in the ray path, usually Quarz, so the birefringence of both superpose and sum or subtract (Boenigk 1983).
For interference figures a condenser lens is inserted in the ray path and all blinds are opened to maximal brightness. Furthermore a so called Bertrand lens is added. By doing so a convergent image develops with concentric colored lines, the isochromats, and black bands (isogyres, Boenigk 1983, Stoiber & Morse 1994). This is used to define the optical character of the mineral.
By investigating these characteristics, the different minerals can be specified with the help of reference books (i.e. Boenigk 1983, Mange & Maurer, H. F. W. 1992). The amount of grains counted per sample was at least N=220. It is recommended to count maximum 300 grains per sample for the best cost-benefit ratio, but the error produced by counting 100 grains is already less than the variability of composition in a sediment layer (Boenigk 1983, Popp *et al.* 2007).

5 Results

The average composition of heavy minerals on Muostakh Island is dominated by hornblende, pyroxene and garnet. Furthermore the samples have a considerable amount of altered grains (in the average 45.1%). Besides the brownish, sometimes greenish, dirty black alterites, shiny red altered aggregates appeared in the samples. These were counted separately for the possibility to be a significant signal of transportation. The average distribution values shown in Fig. 5.1 for the whole sequence excluding altered grains are: 40% for hornblende, 12.2% for pyroxene, 11.2% for garnet, 10.6% for opaque minerals, 7.9% for minerals of the epidot-group (compound by dominating part of epidot and a minor part of zoisite), 6.9% for zircon, 6% for apatite, 2.8% for red aggregates, 1.9% for kyanite and 0.3% for rutile and tourmaline, respectively. Fig. 5.2 shows the average heavy mineral distribution values of the units in a pie chart for each. In all three units the biggest fractions are hornblende, pyroxene, garnet and opaque minerals in changing order. Rutile and tourmaline are a minor fraction in all units. Generally the average heavy mineral distribution in the units show little change. -kleine änderungen nennen

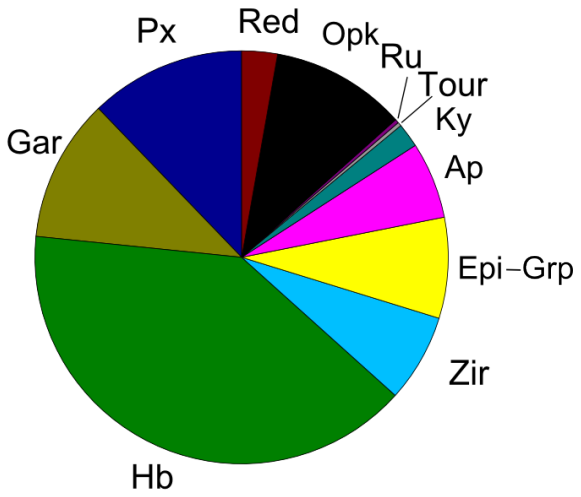

Figure 5.1: Pie chart of the average distribution of heavy minerals of all samples: Px - pyroxene, Gar - garnet, Hb - hornblende, Zir - zircon, Epi-Grp - group of epidot minerals, Ap - apatite, Tour - tourmaline, Ru - rutile, Opk - opaque minerals, Red - red aggregates

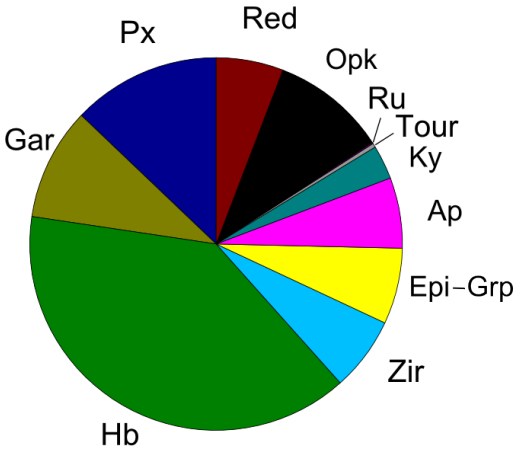

((a)) Unit 1

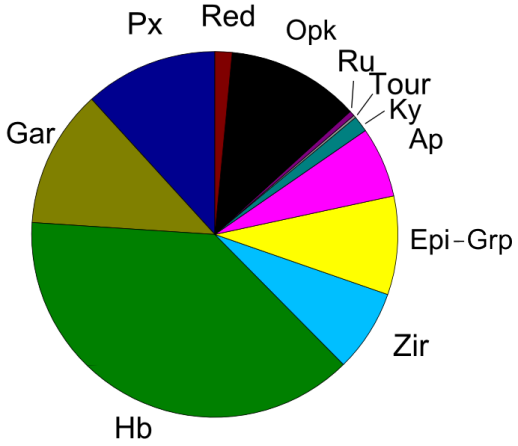

((b)) Unit 2

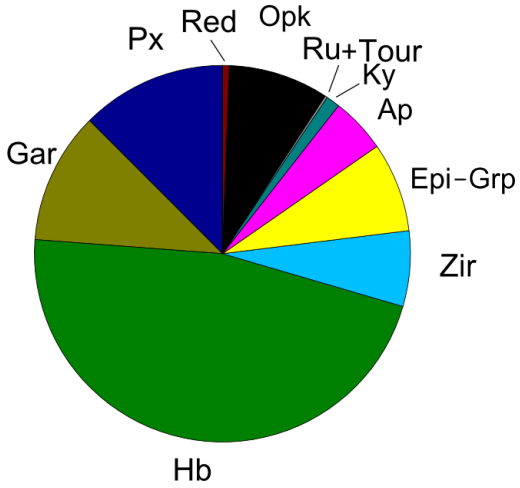

((c)) Unit 3

Figure 5.2: Pie chart of the average distribution of heavy minerals in the three units of the stratigraphic sequence: Px - pyroxene, Gar - garnet, Hb - hornblende, Zir - zircon, Epi-Grp - group of epidot minerals, Ap - apatite, Tour - tourmaline, Ru - rutile, Opk - opaque minerals, Red - red aggregates

Figure 5.3 shows the composition of heavy minerals vs. height over the whole sampled sedimentary sequence. The black striped lines indicate the boundaries of the different stratigraphic units. Unit 1 spreads from ca. 4 m asl till ca. 9 m asl and unit 3 overlays unit 2 at ca. 17 m asl. In the following, the distribution of single minerals with depth is described.

Hornblende is the largest heavy mineral fraction in the samples and represents the group of amphibols. The average relative value for the first unit is 39% ranging between a minimum of 25.9% and a maximum of 45.1%, while the average distribution value in the second unit is 38.4% with a variation between 28.4% and 45.8% and in the third unit at 46.7%. Generally there are just little variations of the amphibol

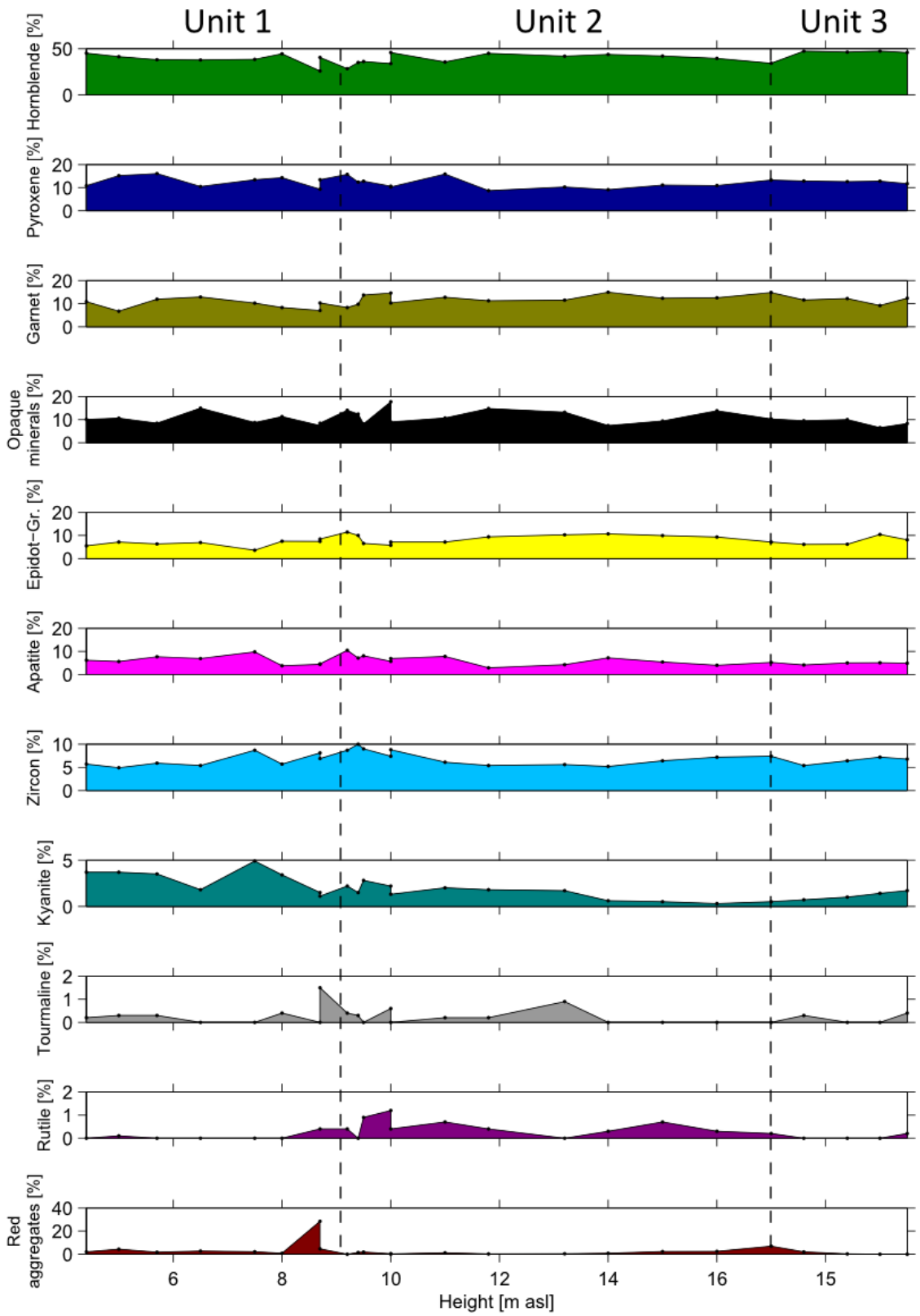

Figure 5.3: Distribution curve of the heavy minerals found in the samples

fraction over the height.

Pyroxene has an average distribution of 12.9% ranging between a minimum of 9.3% and a maximum of 16.1% in the first unit, an average distribution of 11.7% fluctu-

ating between a 8.7% and 15.9% in the second unit and an average distribution of 12.5% varying between 12.9% and 11.7%. The distribution curve of pyroxene can be divided in two parts at ca. 12 m asl of the profile. In the lower part the relative pyroxene contents fluctuate more and has a higher level (12.6%) than in the upper part (11.6%).

Garnet shows in the first unit an average distribution of 9.8% with a fluctuation between 6.7% and 12.9%. The average distribution in the second unit is 12.2% with a fluctuation between 8.3% and 14.9% and in the third unit it is 11.3%. All in all the distribution curve of garnet shows just a slight increasing trend upward from the bottom to the top and displays little variations. Only at 9.5 m asl there exists a distinctive spike.

The opaque minerals have in the first unit an average value of 10% ranging between 7.4% and 15%, while in the second unit the average value is 11.7% ranging between a minimum of 7.4% and a maximum of 17.7%. In the third unit it is 8.6% ranging between a minimum of 6.5% and a maximum of 10%. There is no trend visible, but some distinctive maxima at 6.5 m asl and 10 m asl and a higher fluctuation in the part below ca 10 m asl.

The group of epidot minerals shows in the first unit an average value of 6.6% with a variation between 3.6% and 8.4%. The average value for the second unit is 8.7% ranging between 11.4% and 5.8% and in the third unit the average value is 7.7% ranging between 6.1% and 10.4%. Generally there is no trend over the height but a spike at the boundary between the first and second unit is visible.

The distribution of apatite is in average 6.1% in the first unit ranging between 3.8% and 9.8%. In the second unit the average distribution value is 6.2%, while in the third unit the average value is 4.8% ranging between 4.1% and 5.1%.

Besides the two peaks at 7.5 m asl and 9.2 m asl the value curve is relatively stable.

Zircon has in the first unit an average value of 6.4% ranging between 8.7% and 4.9%. In the second unit the average content of zircon is 7.3% with a fluctuation between 5.2% and 10% and in the third unit it has a distribution value of 6.5% in the average ranging between 5.4% and 7.2%. The distribution curve has a part with a higher level between 7 m asl and 11 m asl compared to the other parts, which are relatively stable and lower values in the upper part.

The distribution curve of kyanite shows a clear separation in two parts. Below the boundary between the first and second unit the heavy mineral values show a higher content of kyanite than above. In the second unit the content decreases further. The average value in the first unit is 3%. In the second unit the average value is 1.4% fluctuating between 2.8% and 0.3%. In the third unit the average distribution value is 1.2%. The absolute minimum is at 16 m asl with 0.3%.

The distribution value of tourmaline is generally very low, in ten samples even no

tourmaline was found. There is no trend visible over the dataset. Just a few peaks appear at 8.7 m asl (1.5%, MUO12-SS-11), at 10 m asl (0.6%, MUO12-SS-08) and at 13.2 m asl (0.9%). The average values for the single units are (from the bottom to the top) 0.3%, 0.2% and 0.2%.

Rutile shows also very low distribution levels close to or equal 0%. It mostly appears just in the second unit with its peak at 10 m asl. The average value for for the units are (from the bottom to the top) 0.1%, 0.5% and 0.05%.

The distribution of the red aggregates is generally very low in the samples. There are just significant peaks at 8.7 m asl with a value of 28.5% and at 17 m asl with a value of 6.9%. The average values are (from the bottom to the top) 5.8%, 1.5% and 0.6%.

All in all the heavy mineral distribution is very uniform over the whole sequence with higher variabilities at the boundaries, especially between the first and second unit.

6 Discussion

6.1 Local interpretation

For a meaningful interpretation the collected heavy mineral data must not only be compared to existing heavy mineral data of the region, but also take into account with other geochemical and further sedimentary data (Diekmann & Kuhn 1999). In this purpose data of grain-size analysis and ^{14}C-dating of the samples from Meyer (unpublished) are used and a principal component analysis was done.
Generally the heavy mineral composition of the investigated samples from Muostakh Island shows little changes over the complete height and thus implies no large-scale change of provenance over the time of sedimentation. Moreover the high content of alterites indicates a short transportation distance, because of their relatively unstable character. In-situ weathering can be most likely excluded, because of the well-conditioned state of the identifiable minerals.
Heavy minerals can be classified due to their chemical and physical stability. Zircon, tourmaline and rutile represent the most stable minerals, while pyroxene, amphibol and garnet represent relatively unstable minerals (Boenigk 1983). Hence, the ratio between the sum of zircon, tourmaline and rutile (ZTR) and the sum of pyroxene and amphibol (Py+Amp), between ZTR and garnet (Gar) and the ZTR index were calculated (see Figure 6.1). The ZTR/Py+Amp-ratio is displayed in Figure 6.1, and shows a maximum at 8.7 m asl beneath the proposed unconformity at ca. 9 m asl, which indicates a higher rate of physical weathering. This is also visible in the ZTR/Gar-ratio. This implies a chemical and physical weathering for the time equivalent to 8.7 m asl. Furthermore a second peak of the ZTR/Py+Amp-ratio appears at 17 m asl, but cannot be verified with the ZTR/Gar-ratio. So chemical weathering for this time can be excluded and another process has took place.
The ZTR index, which is the percentage of zircon, tourmaline and rutile among transparent, nonmicaceous, detrital heavy minerals (Hubert 1962), shows the same peaks at 8.7 m asl and 17 m asl. It is a index for the maturity of a sand stone and indicates higher erosion rates and transportation energy.

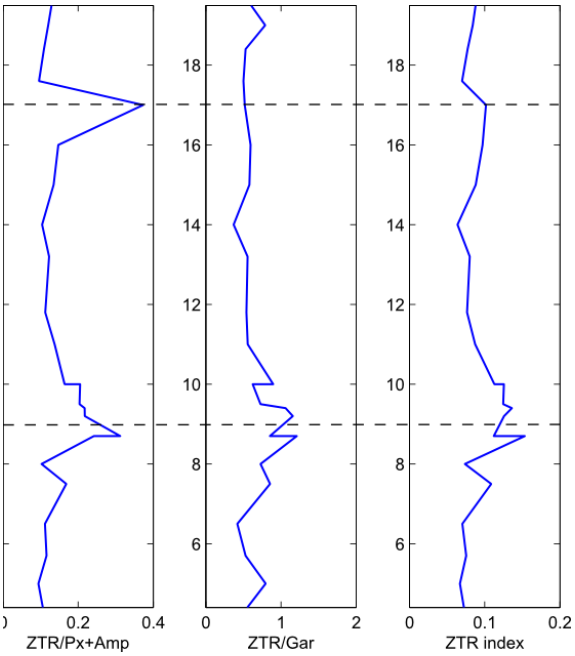

Figure 6.1: left: ratio of sum of zircon, tourmaline and rutile (ZTR) and sum of pyroxene and amphibol (Py+Amp), right: ratio of sum of zircon, tourmaline and rutile (ZTR) and garnet (Gar), the ZTR index was calculate after Hubert (1962), the horizontal black lines indicate the propose boundaries of the stratigraphic units

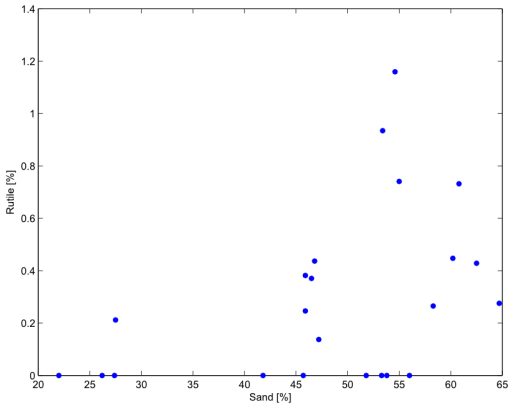

Figure 6.2: Plot showing the relation between the sand fraction and the content of rutil in the investigated samples

Additionally rutile almost just appears in the second unit with a small maximum at the bottom of the unit. The distribution curves of the epidot-group and zircon also show higher values at the bottom of the second unit. Each of them are minerals with a higher density (Ru: 4.23-4.5 g/cm^3, Epi: 5.5-6.5 g/cm^3, Zir: 4.5-4.75 g/cm^3, Boenigk 1983). Hence, they require higher transportation energy. This is also supported by Figure 6.2, which shows that a higher content of rutile just appears in the sediments with a larger sand fraction, which needs also higher energy for transport.

All in all this underlines the assumption of higher transportation energy for the second unit, which is confirmed by the grain-size analysis (see A.2, Meyer (unpublished)).

Above ca. 8.7 m asl the grain-size analysis shows a clear change from a silt-dominated to a sand-dominated composition with a relatively higher content of

gravel until ca. 17 m asl, where the layers are again dominated by silt with nearly no gravel content.

Further the ^{14}C-dating shows a hiatus between ca. 41.6 kyr BP and ca. 19.7 kyr BP in the range from 8.7 m asl to 10 m asl. ^{14}C-dating vs. height also indicates a higher accumulation rate between ca. 10 m asl and ca. 14 m asl (see A.2, Meyer (unpublished)).

However, with the help of principal components analysis (PCA) it is possible to specify three significant signals from the heavy mineral data in combination with the data of grain-size analysis, which are transferred in the sediments and thats loadings are displayed in Figure 6.3 a-c.

The first principle component shows a correlation between the sand sized fraction and the content of rutile and opaque minerals in the samples, which allows the conclusion, that processes, namely changing erosional energy, leading to changes in the grain-size have also an impact on the heavy mineral distribution.

The second principle component shows the impact of the source region on the heavy mineral composition. The load of the grain-size distribution is nearly abundant in this component, while the correlation between pyroxene, zircon, apatite and kyanite on one side against the correlation of hornblende, garnet and the group of epidot minerals on the other side indicate different heavy mineral compositions in the source rocks.

The third principle component represent a signal of chemical weathering. It is strongly influence by the correlation of the red aggregates and zircon. A higher content of the red aggregates can be explained by chemical weathering. In this case the content of zircon also rises, because of its high stability against chemical weathering. Figure 6.3 d shows the three PC vs. the height. Thereby it is easy visible, that PC 1 show similarities to the distribution curve for silt in the cumulative grain-size distribution (see A.2). The curves of PC 2 and PC 3 show little variability. PC 2 has a minimum close to the boundary between unit 1 and unit 2, indicating a sudden change over a short time, while the minimum of PC 3 at the height of the boundary of unit 1 and unit 2 (ca. 9 m asl) indicates the already mentioned chemical weathering.

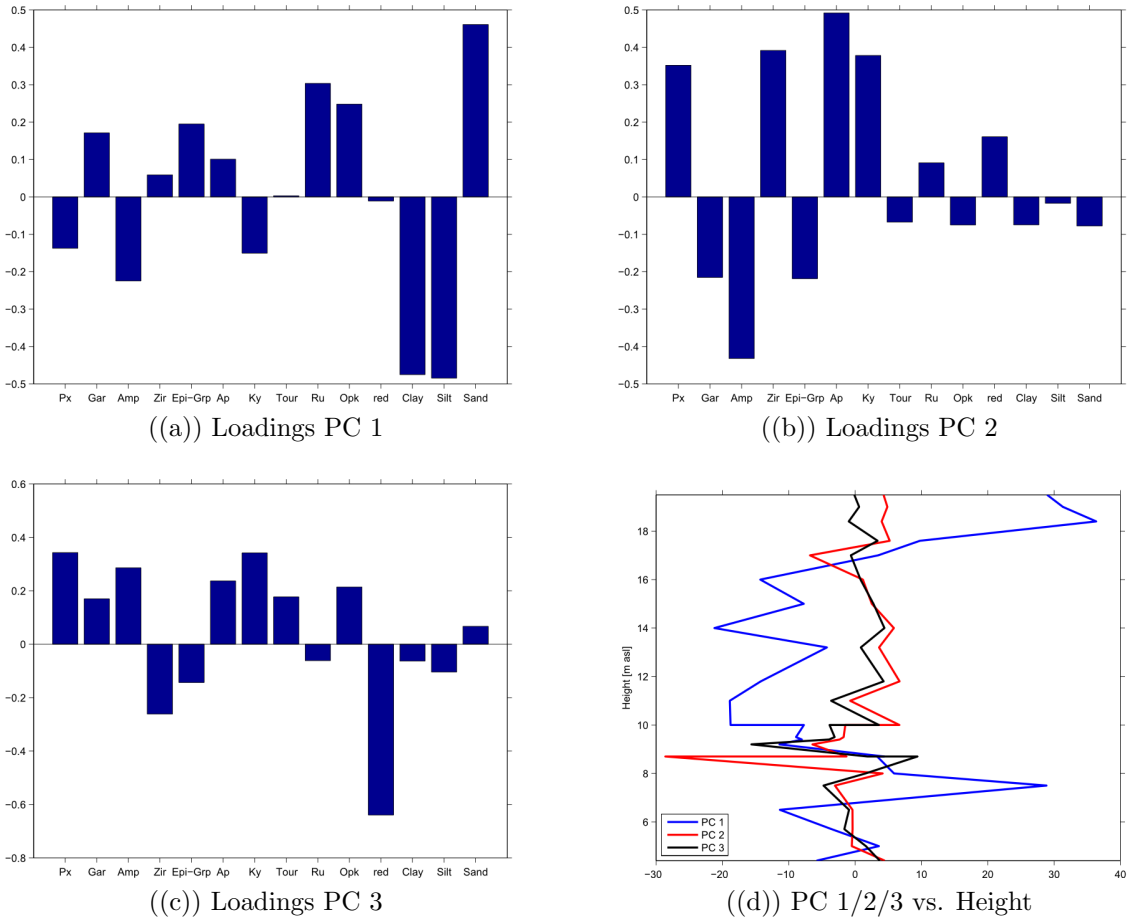

((a)) Loadings PC 1

((b)) Loadings PC 2

((c)) Loadings PC 3

((d)) PC 1/2/3 vs. Height

Figure 6.3: (a, b, c) Loadings of the first, second and third principal component (PC), (d) Plot of the first, second and third principal component vs. height

6.2 Regional interpretation

In order to identify the origin of the deposited material the acquired heavy mineral data has to be compared with regional data sets. Several works for this area has been finished e.g. by Slagoda (1993), Peregovich (1999), Schwamborn *et al.* (2002) and Grosse *et al.* (2007). As potential origin several regions, which are all located on the continental side, were expected. To identify possible areas of origin data sets from the Khorogor Valley, the Darpi river, the Lena Delta, and the Bykovsky Peninsula were used for comparison.

Peregovich (1999) divided Holocene sedimentary deposits of the Laptev Sea from east to west into three areas of different origin. The main influx is driven by the largest rivers - Lena, Yana, Omoloy, Khatanga, Anabar- draining into the Laptev Sea. Muostakh Island lies in a zone of intersection of the Lena provenance and the Yana provenance for heavy minerals (Figure 6.4, Peregovich 1999). The main characteristics of the Lena provenance is a dominating fraction of amphibol influenced by the drainage of the river Lena, while the Yana provenance is dominated by

mica, opaque minerals and alterites influenced by the drainage of the rivers Yana and Omoloy (Peregovich 1999). Schwamborn *et al.* (2002) showed that the heavy mineral composition of the Lena Delta changed just slightly over the Quaternary. All three terraces of the Lena Delta, deposited over the Quaternary, are characterized by amphibol as the largest fraction followed by pyroxene, garnet and epidot in changing order with relatively small changes in the heavy mineral distribution (Schwamborn *et al.* 2002). So it is possible to make assumptions about the heavy mineral provenance of the Pleistocene material with the help of regional Holocene data.

The domination of amphibol in the Holocene marine sediments and the similarities between the late Pleistocene sediments of the Lena Delta and the investigated samples indicate the Lena river as the most possible potential source region. The larger average distribution value for amphibol of the investigated samples compared to the ones from the Lena Delta can be explained with the relatively light density of amphibol (Peregovich 1999). So little energy is needed for a larger distance transport compared to garnet and opaque minerals.

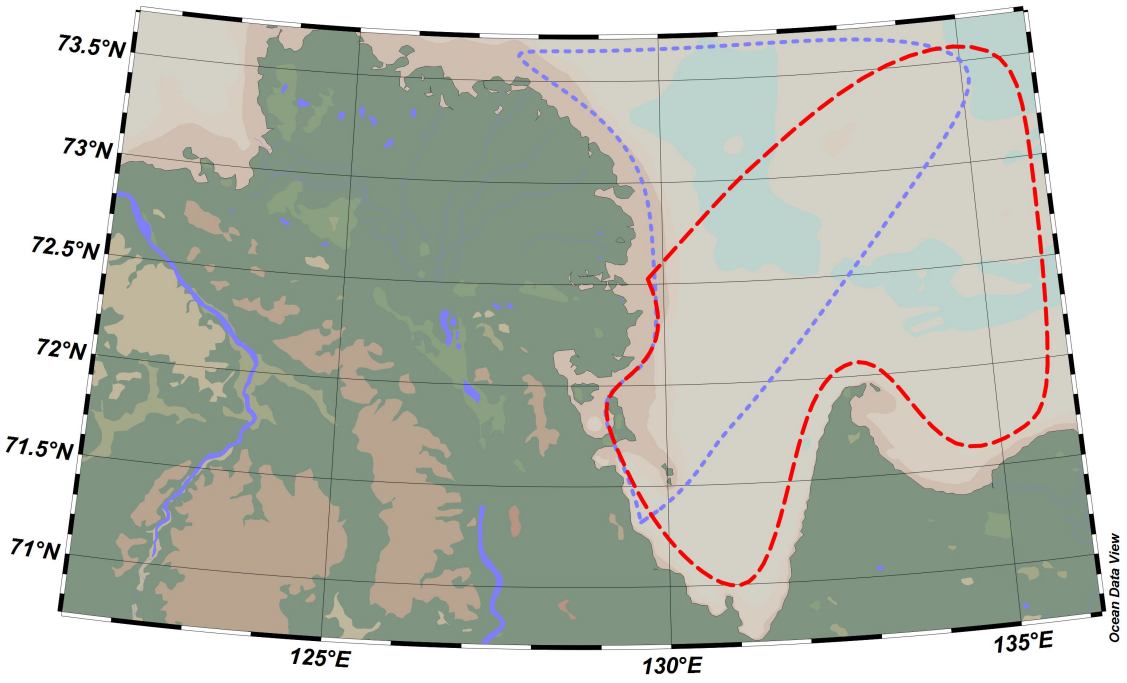

Figure 6.4: Map of study region with Holocene sediment provenance after Peregovich (1999): blue - section of Lena-provenance, red - section of Yana-provenance, map made with Ocean Data View (Schlitzer 2015)

The large amount of alterites could indicate the rivers Omoloy and Yana as another possible origin or a influencing factor. As described by Peregovich (1999) these rivers are responsible for the main influence of heavy mineral composition in the south-eastern Laptev Sea, characterized by a large fraction of alterites, mica and opaque

minerals. Because of the greater distance of Yana to the study region Omoloy is the more possible potential heavy mineral source area. But generally the amount of opaque minerals in the investigated samples is less than in samples of the Lena Delta, which is not mainly dominated by opaque minerals. Also no mica was found in the investigated samples. In this purpose the influence of Omoloy can be excluded or rated on a minimum.

Another possible source region for the material of Muostakh Island is the Khorogor Valley, which is suggested by Grosse *et al.* (2007) as origin for sediments on the Bykovsky Peninsula. This can be definitely excluded as a potential source region. Heavy mineral compositions of different researchers show there a domination of pyroxene with ca. 30 - 40% followed by leucoxen and opaque minerals in the Khorogor Valley area. Amphibol, epidot and garnet, which are widely dominant in the region, are just present in small amounts (Slagoda 1993, Peregovich 1999, Schwamborn *et al.* 2002, Grosse *et al.* 2007, Schirrmeister *et al.* 2011). Furthermore leucoxen, as characteristic for the Khorogor Valley area, could not be identified in the investigated samples of Muostakh Island. Grosse *et al.* (2007) also describes a change of the grain-size distribution on the Bykovsky Peninsula, which can also be seen in the data of heavy mineral composition (e.g. Slagoda 1993). The heavy mineral composition of Muostakh Island and Bykovsky Peninsula suggest that another sedimentological boundary has to be considered between this places.

The Khara-Ulakh ridge in general is another possible source region. Data from Christine Siegert (personal communication) are used as representatives for the ridge. This suggest, that the mountain ridge influenced the heavy mineral composition on the Bykovsky Peninsula, in order of pyroxene and amphibol content, but not the Muostakh Island.

Figure 6.5 shows heavy mineral compositions in the region of the third terrace of the Lena Delta, of the Bykovsky Peninsula, the Khorogor valley, the valley of the river Darpi and of the Muostakh Island. This shows clear a lightly confusing situation. The material for Muostakh Island seems transported over the today's sea side and not influenced by sedimentation processes in the Khara Ulakh ridge, while the narrow Bykovsky Peninsula show influences of the Khara Ulakh ridge, namely from the Khorogor Valley and also possibly the region around the river Darpi.

Morton & Hallsworth (1999) defined ratios between heavy minerals with similar density and grain size as good provenance indicators, which are more independent of hydraulics and burial diagenesis. Pyroxene and amphibol fulfill this requirements (Boenigk 1983). The ratio between pyroxene and amphibol in the average is ca. 0.3 for the investigated samples which is relatively similar to the ratio (ca. 0.6) of the samples of the third terrace of the Lena Delta taken by Schwamborn (2002).
Figure 6.6 shows the ratio between Pyroxene and Amphibol of the data displayed in Figure 6.5. Thereby three provenance of the region can be identified as one provenance with a relatively high amphibol content and a relatively low pyroxene content (Lena-provenance), one provenance with a relatively high pyroxene content and a relatively low amphibol content (Khorogor Valley-provenance) and a provenance of intermediate values (Darpi-provenance). The investigated sample can be easily allocated to the Lena-provenance.

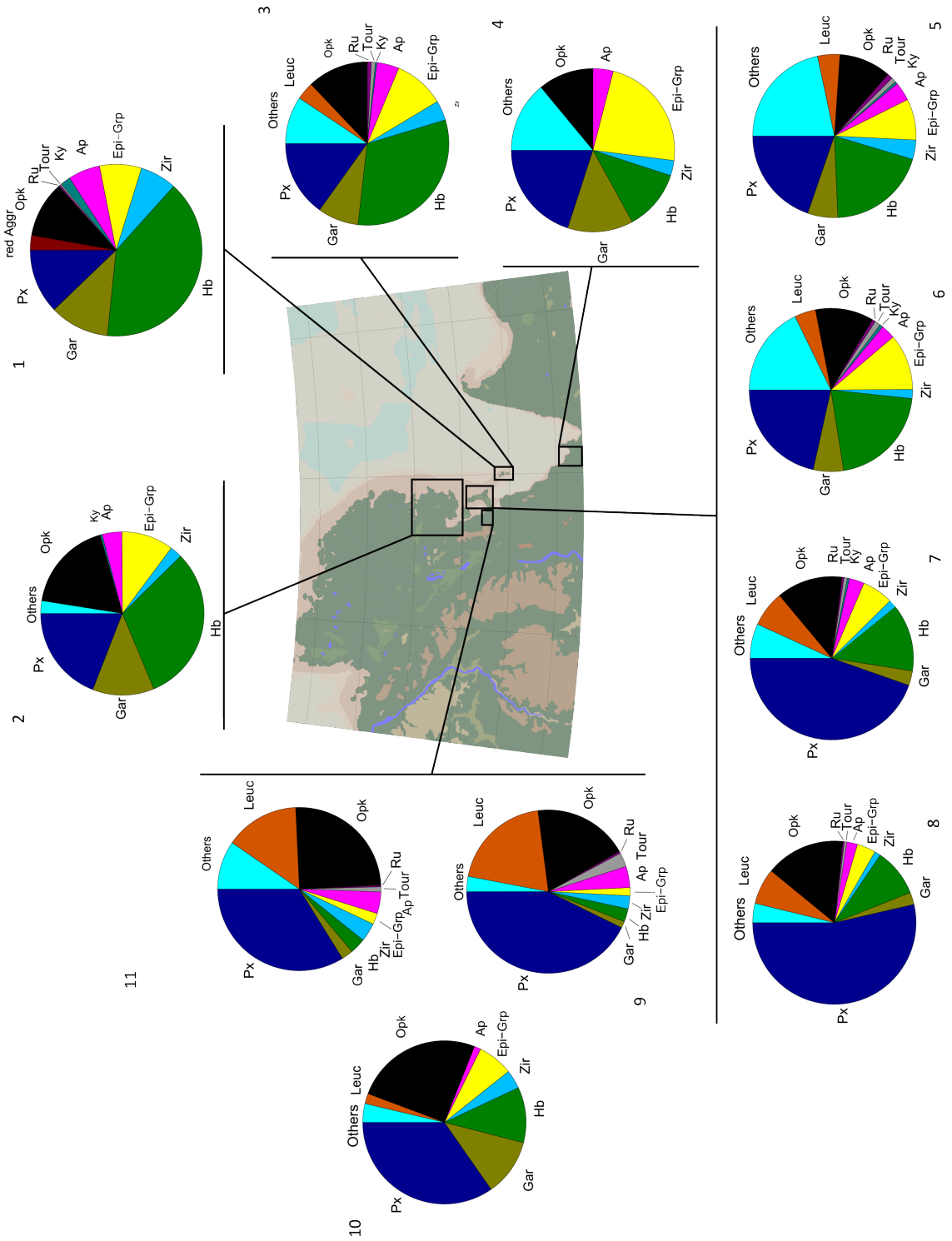

Figure 6.5: Map showing heavy mineral composition in the region: 1 - average composition of investigated samples, 2 - third terrace of Lena Delta, Schwammborn (2002), 3 - Muostakh Island, Slagoda (1993), 4 - Khara Ulakh, Christine Siegert (personal communication), 5 - outcrop "Mamontovy", Schirrmeister *et al.* (2011), 6 - outcrop "Mamontovy", Schirrmeister *et al.* (2011), 7 - outcrop "Mamontovy", Slagoda (1993), 8 - outcrop "Cape Razdelny", Slagoda (1993), 9 - drilling hole X-89, Slagoda (1993), 10 - Khorogor Valley, Christine Siegert (personal communication), 11 - Khorogor Valley, Grosse **et al.** (2007), map made with Ocean Data View (Schlitzer 2015)

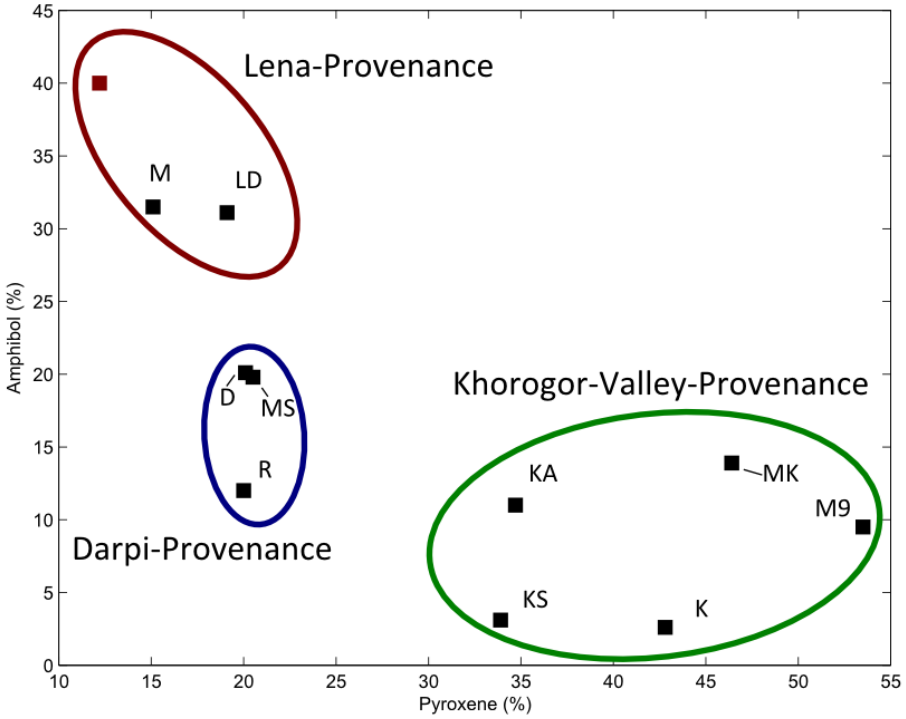

Figure 6.6: Plot Pyroxene vs. Amphibol of investigated sample and comparable data in the region, indicating three provenances for the for Bykovsky Peninsula and Muostakh Island, red - Lena-provenance, blue - Darpi-provenance, green - Khorogor-Valley-provenance, red square - average ratio of investigated samples, D - Darpi river, Christine Siegert (personal communication), K - Khorogor Valley, Grosse *et al.* (2007), KA - Khorogor Valley, Christine Siegert (personal communication), KS - Khorogor Valley (drilling hole X-89), Slagoda (1993), LD - Lena Delta third terraces, Schwamborn (2002), M - Muostakh Island, Slagoda (1993), M9 - Bykovsky Peninsula (outcrop "Mamontovy"), Schirrmeister *et al* (2011), MS - Bykovsky Peninsula (outcrop "Mamontovy"), Slagoda (1993), MK - Bykovsky Peninsula (outcrop "Mamontovy"), Grosse *et al.* (2007), R - Bykovsky Peninsula (outcrop "Cape Razdelny", Slagoda (1993)

7 Conclusion

This thesis used a microscopic heavy mineral analysis to identify the provenance of the sedimentary material of the Ice Complex formation on Muostakh Island. The method gave a clear result to interpret. It was possible to give an interpretation about the origin, transportation energy and chemical weathering of the sediment as effects influencing the heavy mineral composition, which was furthermore possible to confirm in combination with grain-size distribution data, ^{14}C-dating and principal component analysis.

The Ice Complex sequence from Muostakh Island, divided in three stratigraphic units, consists mainly of sediments of sandy silt to silty sand and peat layers from the late Pleistocene. Between the first and second unit a hiatus from ca. 41.6 kyr BP to ca. 19.7 kyr BP exists, which is indicated by an erosional plane and proved by ^{14}C-dating.

The heavy mineral composition is dominated by amphibol, pyroxene, garnet and opaque minerals. Further minerals of the epidot-group, zircon, apatite and kyanite appeared, while rutile and tourmaline are accessory present. Beside a huge amount of dark alterites a red shiny aggregate was found, indicating chemical weathering at significant points. Generally the composition show little change over the whole sequence, but with principal component analysis a link between the grain-size distribution and the amount of rutile and opaque minerals and a singular chemical weathering process could be shown.

As origin the river Lena can be identified, because of similarities of the heavy mineral composition of the Lena Delta terraces and the Lena influenced Holocene marine sediments. Thereby the Khorogor Valley and other parts of the Khara Ulakh ridge can be excluded as pathways of the sediment to its current settlement.

More specific information can be gained by a further investigation of the opaque minerals of the heavy mineral fraction and clay minerals of the sediment. The pathway of the material from its source to its settlement should still be discussed. Whether it came from the Lena Delta over the today's seaside or another unknown pathway in the Khara Ulakh ridge. However, the geological situation in this study region seems a bit confusing, because of the influence of different areas on locations of settlement with way more narrow distances between each other.

8 Bibliography

Bauch, H. A., Kassens, H., Erlenkeuser, H., Grootes, P. M., & Thiede, J. 1999. Depositional environment of the Laptev Sea (Arctic Siberia) during the Holocene. *Boreas*, 194–204.

Bauch, H.A, Mueller-Lupp, T., Taldenkova, E., Spielhagen, R.F, Kassens, H., Grootes, P.M, Thiede, J., Heinemeier, J., & Petryashov, V. V. 2001. Chronology of the Holocene transgression at the North Siberian margin. *Global and Planetary Change*, **31**(1-4), 125–139.

Behrends, M. 1999. Rekonstruktion von Meereisdrift und terrigenem Sedimenteintrag im Spätquartär Schwermineralassoziationen in Sedimenten des Laptev-See-Kontinentalrandes und des zentralen Arktischen Ozeans. *Berichte Polarforschung*.

Boenigk, W. 1983. *Schwermineralanalyse*. Stuttgart: Ferdinand Enke Verlag.

Brown, J., Ferrians O. J. Jr., Heginbottom, J. A., & Melnikov, E. S. 1998. *Circum-Arctic Map of Permafrost and Ground-Ice Conditions*.

Diekmann, B., & Kuhn, G. 1999. Provenance and dispersal of glacial–marine surface sediments in the Weddell Sea and adjoining areas, Antarctica: ice-rafting versus current transport. *Marine Geology*, **158**(1-4), 209–231.

Drachev, S. S., Savostin, L. A., Groshev, V. G., & Bruni, I. E. 1998. Structure and geology of the continental shelf of the Laptev Sea, Eastern Russian Arctic. *Tectonophysics*, **298**(4), 357–393.

French, H. M. 1996. *The periglacial environment*. 2nd ed edn. London: Longman.

Galabala, R. O. 1997. Pereletki and the initiation of glaciation in Siberia. *Quaternary International*, **41-42**, 27–32.

Gravis, G.F. 1969. Slope deposits in Yakutia. 1–128.

Grigoriev, M. N. 1993. Cryomorphogenesis of the Lena River mouth area. *Russian Academy of Science, Siberian Branch, Yakutsk, Russia*.

Grosse, G., Schirrmeister, L., Siegert, C., Kunitsky, V. V., Slagoda, E. A., Andreev, A. A., & Dereviagyn, A. Y. 2007. Geological and geomorphological evolution of a sedimentary periglacial landscape in Northeast Siberia during the Late Quaternary. *Geomorphology*, **86**(1-2), 25–51.

Grosswald, M. G. 1998. Late-Weichselian ice sheets in Arctic and Pacific Siberia. *Quaternary International*, **45-46**, 3–18.

Günther, F., Overduin, P. P., Baranskaya, A., Opel, T., & Grigoriev, M. N. 2013a. Observing Muostakh Island disappear: erosion of a ground-ice-rich coast in response to summer warming and sea ice reduction on the East Siberian shelf. *The Cryosphere Discussions*, **7**(4), 4101–4176.

Günther, F., Overduin, P. P., Sandakov, A. V., Grosse, G., & Grigoriev, M. N. 2013b. Short- and long-term thermo-erosion of ice-rich permafrost coasts in the Laptev Sea region. *Biogeosciences*, **10**(6), 4297–4318.

Higgins, C. G., & Coates, D. R. 1990. *Groundwater geomorphology: The role of subsurface water in earth-surface processes and landforms*. Vol. 252. Boulder, Colo.: Geological Society of America.

Holmes, M. L., & Creager, J. S. 1974. Holocene History of the Laptev Sea Continental Shelf. *Pages 211–229 of:* Herman, Y. (ed), *Marine Geology and Oceanography of the Arctic Seas*. Springer Berlin Heidelberg.

Hubert, J. F. 1962. A Zircon-Tourmaline-Rutile Maturity Index and the Interdependence of the Composition of Heavy Mineral Assemblages with the Gross Composition and Texture of Sandstones.

Karte, J. 1979. Entwicklung und gegenwärtiger Stand der deutschen Periglaziärforschung in den polaren und subpolaren Regionen. *Polarforschung*, 97–115.

Kloss, A. L. 2008. Water isotope geochemistry of recent precipitation in Central and North Siberia as a proxy for the local and regional climate system.

Mange, M. A., & Maurer, H. F. W. 1992. *Heavy Minerals in Colour*. London: Chapman & Hall.

Meyer, H., Dereviagyn, A. Y., Siegert, C., Schirrmeister, L., & Hubberten, H.-W. 2002. Palaeoclimate reconstruction on Big Lyakhovsky Island, north Siberia?hydrogen and oxygen isotopes in ice wedges. *Permafrost and Periglacial Processes*, **13**(2), 91–105.

Meyer, H., Opel, T., Laepple, T., Dereviagyn, A. Y., Hoffmann, K., & Werner, M. 2015a. Long-term winter warming trend in the Siberian Arctic during the mid- to late Holocene. *Nature Geosci*, **8**(2), 122–125.

Meyer, H., Opel, T., & Derevyagin, A. 2015b. Stratigraphic and Sedimentological Studies. *Pages 79–82 of:* Bornemann, H. (ed), *Russian-German cooperation system Laptev Sea : the expedition LENA 2012*. Reports on polar and marine research, Bremerhaven, Alfred Wegener Institute for Polar and Marine Research.

Morton, A. C., & Hallsworth, C. R. 1994. Identifying provenance-specific features of detrital heavy mineral assemblages in sandstones. *Sedimentary Geology*, **90**(3-4), 241–256.

Morton, A. C., & Hallsworth, C. R. 1999. Processes controlling the composition of heavy mineral assemblages in sandstones. *Sedimentary Geology*, **124**(1-4), 3–29.

Müller, C., & Stein, R. 2000. Variability of fluvial sediment supply to the Laptev Sea continental margin during Late Weichselian to Holocene times: implications from clay-mineral records. *International Journal of Earth Sciences*, **89**(3), 592–604.

Nagaoka, D., Saijo, K., & Kukuda, M. 1995. Sedimental environment of the Edoma in high Arctic eastern Siberia. *Proceedings of the Third Symposium on the joint Siberian permafrost Studies between Japan and Russia in*, **1994**, 8–13.

Peregovich, B. 1999. Die postglaziale Sedimentationsgeschichte der Laptewsee: schwermineralogische und sedimentpetrographischeUntersuchungen. **1999**.

Popp, S., Belolyubsky, I., Lehmkuhl, F., Prokopiev, A., Siegert, C., Spektor, V., Stauch, G., & Diekmann, B. 2007. Sediment provenance of late Quaternary morainic, fluvial and loess-like deposits in the southwestern Verkhoyansk Mountains (eastern Siberia) and implications for regional palaeoenvironmental reconstructions. *Geological Journal*, **42**(5), 477–497.

Rozenbaum, G. E. 1981. Special features of lithogenesis of the alluvial planes in the Eastern Subarctic as related to the problem of the Ice (Yedoma) Complex. *Problems of cryolithology*, 87–100.

Schirrmeister, L., Siegert, C., Kunitzky, V. V.., Grootes, P. M., & Erlenkeuser, H. 2002. Late Quaternary ice-rich permafrost sequences as a paleoenvironmental archive for the Laptev Sea Region in northern Siberia. *International Journal of Earth Sciences*, **91**(1), 154–167.

Schirrmeister, L., Kunitsky, V., Grosse, G., Wetterich, S., Meyer, H., Schwamborn, G., Babiy, O., Derevyagin, A., & Siegert, C. 2011. Sedimentary characteristics and

origin of the Late Pleistocene Ice Complex on north-east Siberian Arctic coastal lowlands and islands – A review. *Quaternary International*, **241**(1-2), 3–25.

Schirrmeister, L., Froese, D., Tumskoy, V., Grosse, G., & Wetterich, S. 2013. PERMAFROST AND PERIGLACIAL FEATURES — Yedoma: Late Pleistocene Ice-Rich Syngenetic Permafrost of Beringia. *Pages 542–552 of: Encyclopedia of Quaternary Science*. Elsevier.

Schlitzer, R. 2015. *Ocean Data View*.

Schwamborn, G., Rachold, V., & Grigoriev, M. N. 2002. Late Quaternary sedimentation history of the Lena Delta. *Quaternary International*, **89**(1), 119–134.

Shahgedanova, M. 2002. *The physical geography of northern Eurasia*. 3 edn. Oxford regional environments. Oxford and New York: Oxford University Press.

Sher, A. V., Kaplina, T. N., & Ovander, O. G. 1987. Unified regional stratigraphic chart for the Quaternary deposits in the Yana-Kolyma lowland and its mountainous surroundings. Explanatory Note. *Decisions of Interdepartmental Stratigraphic Conference on the Quaternary of the Eastern USSR.*, **1982**.

Slagoda, Elena A. 1993. *Genesis i mikrostroenie kriolitogennykh otlozhenii Bykovskogo polyostrova i ostrova Muoastakh [Genesis and microstructure of cryolithogenic deposits at the Bykovsky Peninsula and the Muostakh Island]*. Ph.D. thesis, Russian Academy of Science, Siberian Branch.

Stoiber, Richard E., & Morse, Stearns A. 1994. *Crystal identification with the polarizing microscope*. New York: Chapman & Hall.

Tomirdiaro, S. V., & Chernenky, V. I. 1987. Cryogenic deposits of East Arctic and Sub Arctic. 1–196.

Tucker, M. (ed). 1996. *Methoden der Sedimentologie: 38 Tabellen*. Stuttgart: Enke.

Williams, P. J. 1961. Climatic Factors Controlling the Distribution of Certain Frozen Ground Phenomena. *Geografiska Annalar*, 339–347.

Zhang, T., Barry, R. G., Knowles, K., Heginbottom, J. A., & Brown, J. 1999. Statistics and characteristics of permafrost and ground–ice distribution in the Northern Hemisphere 1. *Polar Geography*, **23**(2), 132–154.

graphicx

A Appendix

A.1 Transgression in Laptev Sea

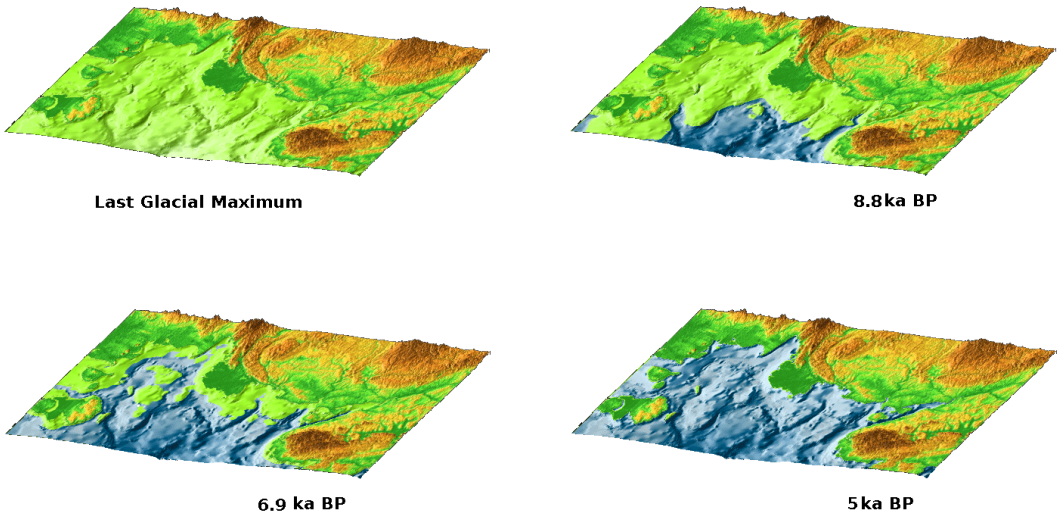

Figure A.1: Transgression in the Laptev Sea to the present state from LGM till 5 ka BP, image modified after Bauch *et al.* (2001)

A.2 External Data

A.2.1 Correlation of δ^{14}C-age and height

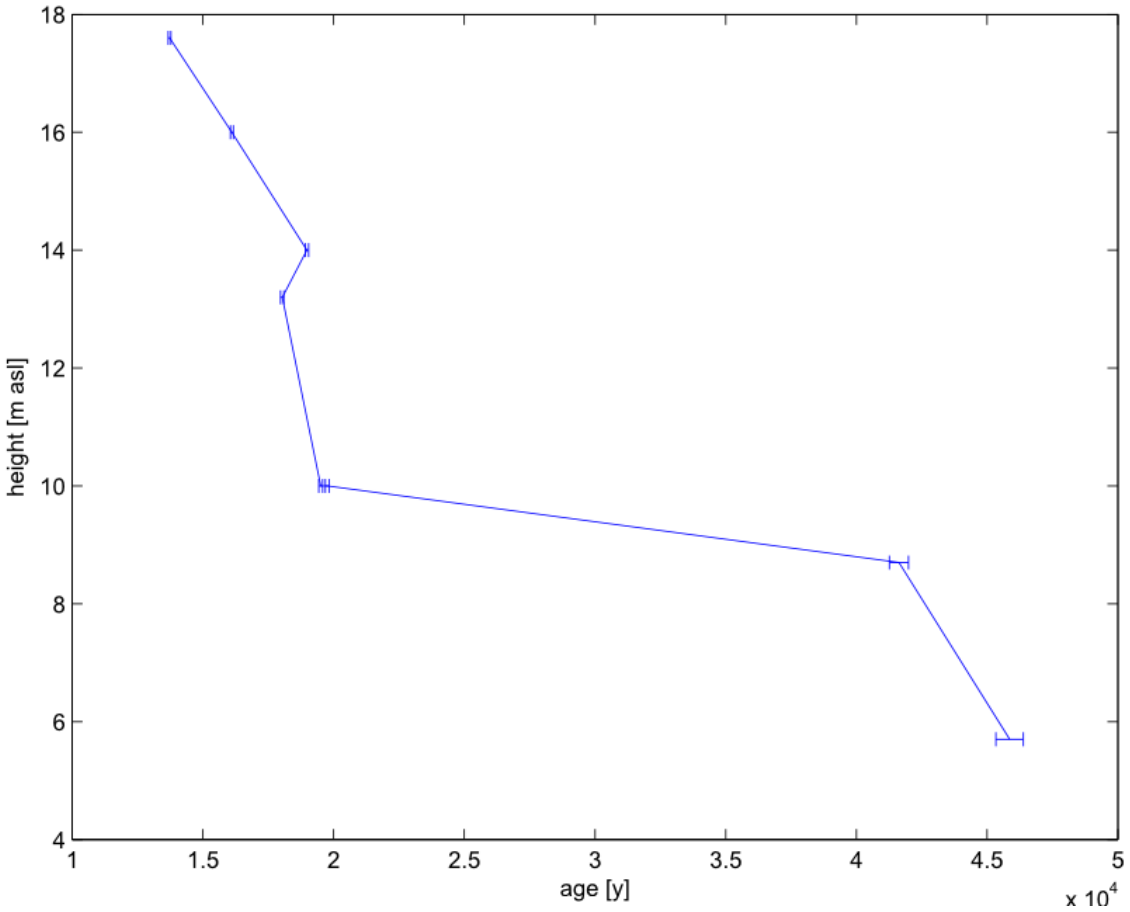

Figure A.2: Correlation between δ^{14}C-age and height, data from Hanno Meyer

Table A.1: ^{14}C-Data from Hanno Meyer

Sample-ID	Height [m asl]	age [y]	$\pm[y]$
MUO12-SS-2	5.7	45860	527
MUO12-SS-8	10	19760	70
MUO12-SS-11	8.7	41626	366
MUO12-SS-13	10	19510	74
MUO12-SS-16	13.2	18036	63
MUO12-SS-20	17.6	13727	50
MUO12-SS-22	16	16108	57
MUO12-SS-24	14	18681	65

A.2.2 Grainsize analysis

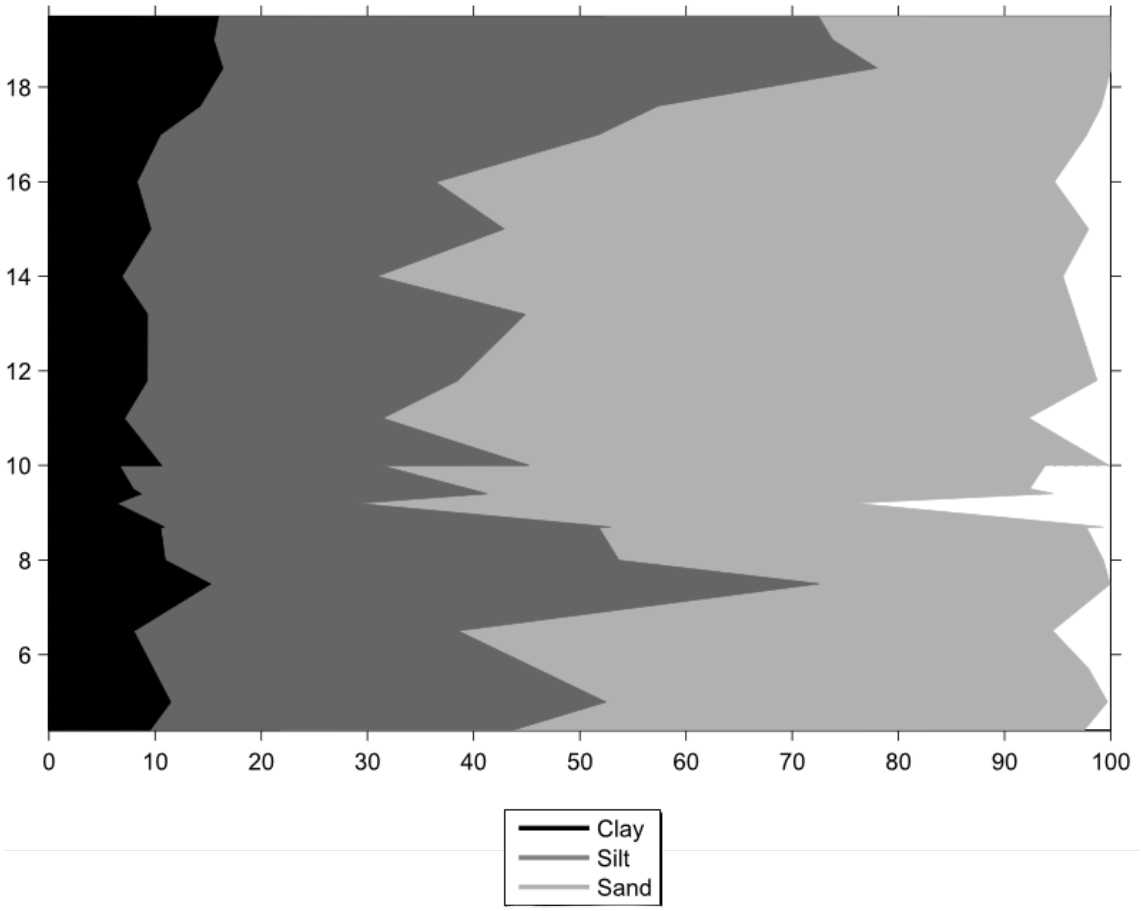

Figure A.3: Grainsize distribution vs. height, data from Hanno Meyer

Table A.2: Grain-size distribution, data from Hanno Meyer

Sample-ID	Height [m asl]	Clay [%]	Silt [%]	Sand [%]
MUO12-SS-01	5	11.5	41	47.2
MUO12-SS-02	5.7	9.9	36.2	51.8
MUO12-SS-03	6.5	8	30.5	56
MUO12-SS-04	4.4	9.5	34.2	53.8
MUO12-SS-05	7.5	15.3	57.3	27.4
MUO12-SS-06	8	10.9	42.7	45.7
MUO12-SS-07	9.5	7.9	31	53.4
MUO12-SS-08	10	10.6	34.7	54.6
MUO12-SS-09	8.7	10.8	42.1	46.5
MUO12-SS-10	9.2	6.3	22.6	46.8
MUO12-SS-11	8.7	10.5	41.3	45.9
MUO12-SS-12	9.4	8.7	32.6	53.3
MUO12-SS-13	10	6.6	25	62.5
MUO12-SS-14	11	7.1	24.3	60.8
MUO12-SS-15	11.8	9.3	29.2	60.2
MUO12-SS-16	13.2	9.3	35.6	51.8
MUO12-SS-17	19.5	16	56.5	27.5
MUO12-SS-18	19	15.5	58.3	26.2
MUO12-SS-19	18.4	16.4	61.6	22
MUO12-SS-20	17.6	14.2	43.1	41.8
MUO12-SS-21	17	10.5	41.3	45.9
MUO12-SS-22	16	8.3	28.1	58.3
MUO12-SS-23	15	9.6	33.3	55
MUO12-SS-24	14	6.9	24	64.7

A.3 Description of heavy minerals

The following is based on observations of the work at the microscope. These are no complete descriptions for the minerals in general. They just describe the appearance of the minerals in the samples. For more detailed descriptions see Mange & Maurer (1992) and Boenigk (1983). It has to be attended that some colors under single-polarized light, interference colors and pleochroism can vary with the thickness or chemical composition of the grains.

A.3.1 Apatite

The grains of apatite minerals appear as well rounded mostly elongated grains. Under single-polarized light they are colorless without showing pleochroism. Under crossed polarization filter they show a weak birefringence and pale gray interference colors of first order. Their extinction is parallel. The grains of apatite are good to recognize due to its shape, weak birefringence and negative elongation. By adding a second refracting material, for instance quartz, the grains become blue or orange depending on their position to the polarizer and analyzer.

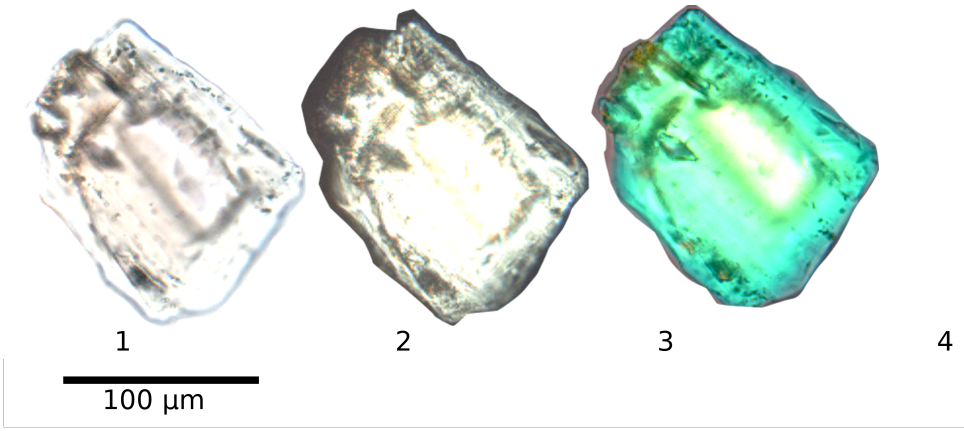

Figure A.4: Microscopy pictures of apatite: (1) single-polarized light, (2) crossed polarization filter, (3) elongation (addition), (4) elongation (subtraction)

A.3.2 Clinopyroxene

The grains of the group of clinopyroxene are mostly elongated, colorless with a pale green undertone under single-polarized light and have a high light refraction. They are mostly very angular and shattered. With crossed polarization filter they show a moderate to strong birefringence and their extinction is symmetric. They show interference colors up to the second order, but also appear with lower interference colors of the first order.

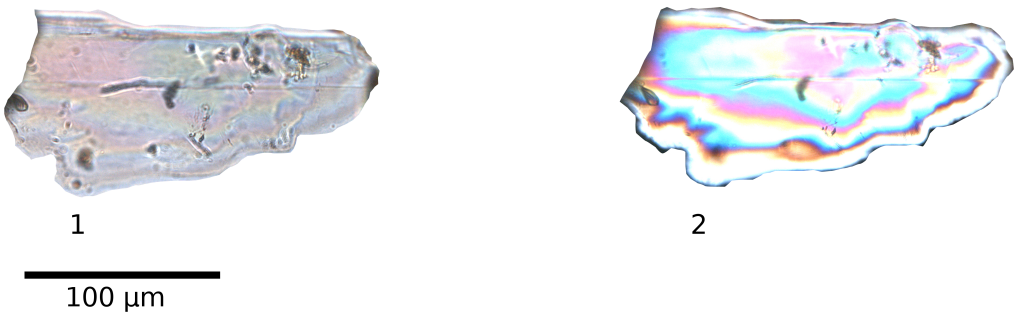

Figure A.5: Microscopy pictures of clinopyroxene: (1) single-polarized light, (2) crossed polarization filter

A.3.3 Epidot

Epidot mainly appears as irregular angular grains with greenish undertone comparable to pistachio green and sometimes with a brown marks of alteration. The grains usually show weak pleochroism between yellowish green and pistachio green. The interference colors are moderate up to the second order with abnormal colors, mostly blue. Under crossed polarization filter they show a almost parallel extinction. The elongation varies.

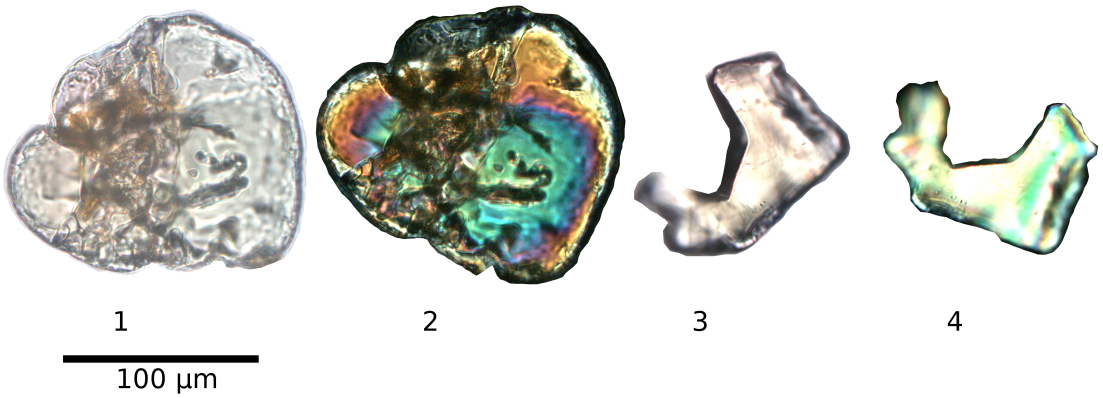

Figure A.6: Microscopy picture of epidot: (1) single-polarized light, (2) crossed polarization filter, (3) single-polarized light, (4) crossed polarization filter

A.3.4 Garnet

This mineral appears as irregular, angular grains with a high relief, but sometimes they are also moderately rounded. It has a high birefringence and under single-polarized light the grains are mostly colorless and sometimes reddish. Garnet shows no interference colors under crossed polarization filter due to its isotropic character.

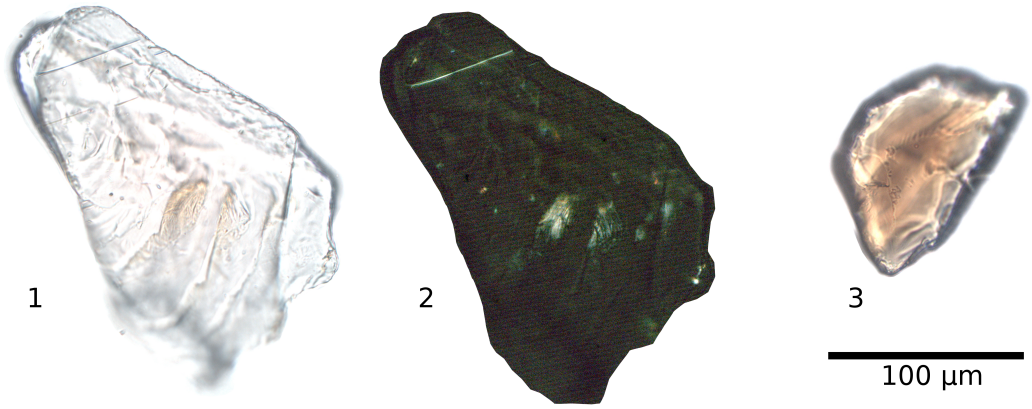

Figure A.7: Microscopy pictures of garnet: (1) single-polarized light, (2) crossed polarization filter, (3) single-polarized light

A.3.5 Hornblende

Grains of the hornblende series appear usually prismatic in green, bluish green or brown. The show strong pleochroism from green to bluish or from light to dark brown. Mostly they have well developed cleavages. Their extinction is almost parallel to parallel and they show a positiv elongation by adding a second refracting material besides activated polarizer and analyzer.

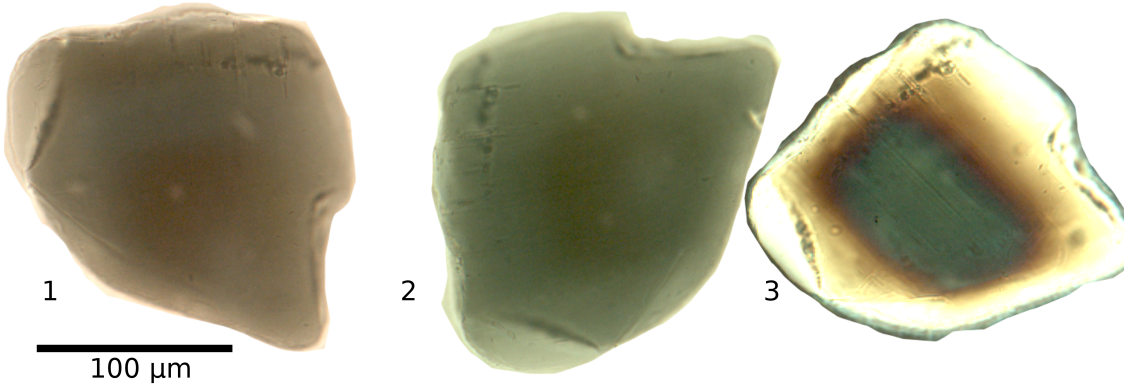

Figure A.8: Microscopy pictures of hornblende: (1) single-polarized light, (2) single-polarized light, 90° rotation, (3) crossed polarization filter

A.3.6 Kyanite

Kyanite mostly shows elongated, bladed and moderately rounded grains. They are mainly colorless with a weak blue tint. With crossed polarization filter kyanite shows low interference colors of the first order and has mostly an oblique extinction. The elongation is positive, what makes it easy to distinguish from apatite.

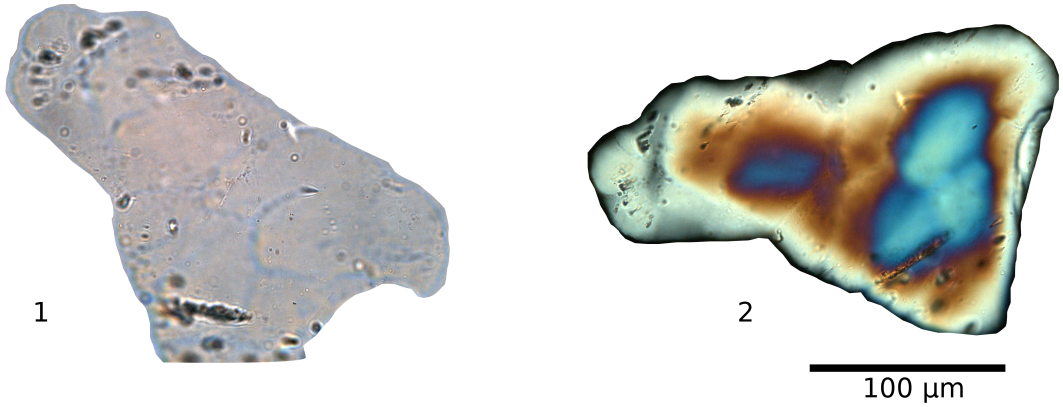

Figure A.9: Microscope pictures of kyanite: (1) single-polarized light, (2) crossed polarization filter

A.3.7 Orthopyroxen

The group of orthopyroxenes is represented by hypersthene. This mineral appears as elongated, mostly well rounded grains with a low sphericity. It shows pleochrosim of different intensity from pale green to pale red. Furthermore it extinct parallel under crossed polarization filter and has positiv elongation. Interference colors are mainly of first order.

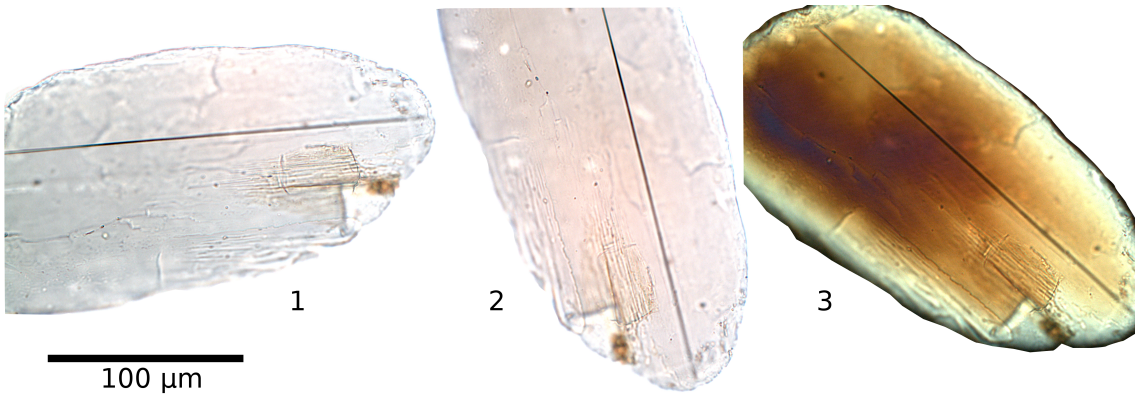

Figure A.10: Microscopy pictures: (1) and (2) single-polarized light, (3) crossed polarization filter

A.3.8 Red Aggregate

The red aggregates appear mostly as angular to subrounded grains and are often fractured. Under single-polarized light they show a specific shiny red, pale brown color. Under crossed polarization filter they are isotrop and show no interference color.

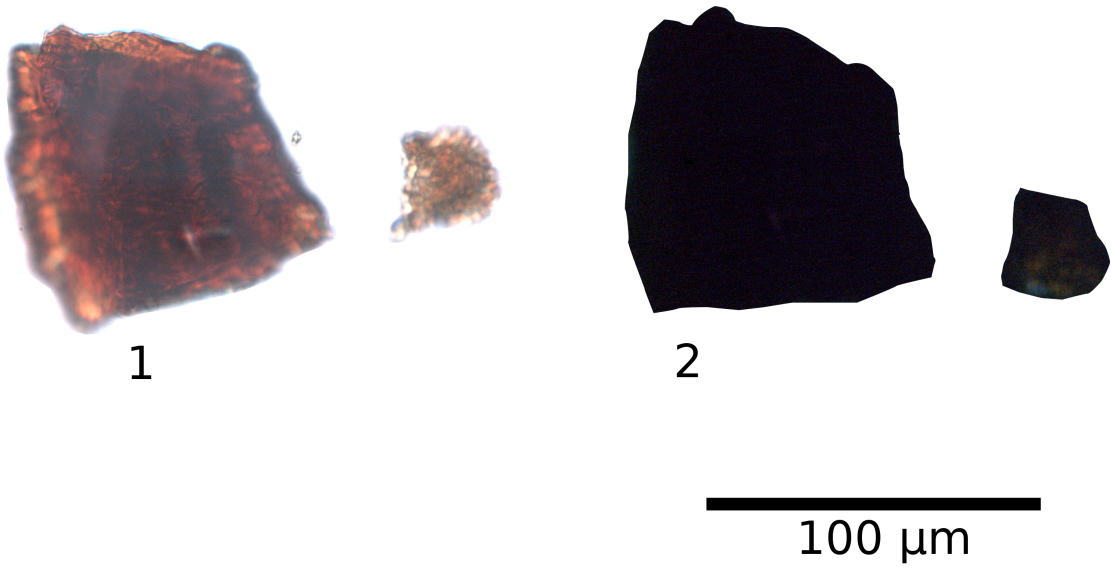

Figure A.11: Microscope pictures of red aggregates: (1) single-polarized light, (2) crossed polarization filter

A.3.9 Rutile

Rutile appears mostly as dark brown well rounded grains with a low sphericity. It has a high refraction which leads to the typical thick black halo around the grains. There are hardly a pleochroism, interference colors, which are in high order and tinted by the color of the grain itself, and elongation to observe. The extinction is parallel.

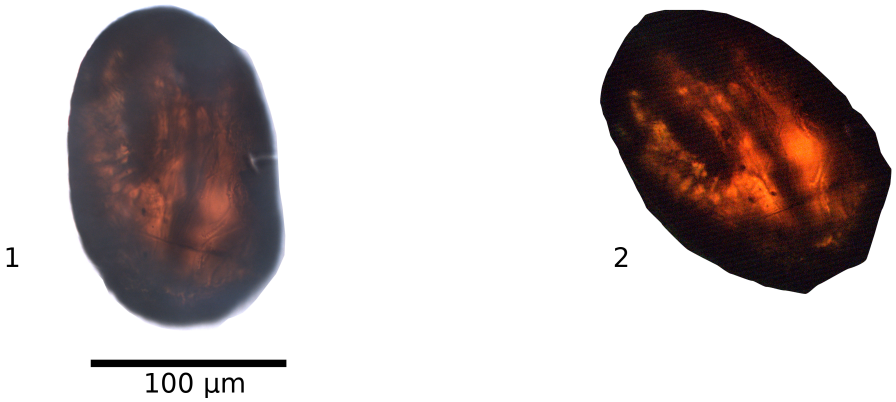

Figure A.12: Microscopy picture of rutile: (1) single-polarized light, (2) crossed polarization filter

A.3.10 Tourmaline

The grains of tourmaline are reddish brown, well rounded and have a high sphericity. Tourmaline has a high birefringence and high interference colors up to the third order, which are deeply tinted according to the strong color. The extinction is parallel and the elongation is hard to observe. Furthermore the grains show no pleochroism.

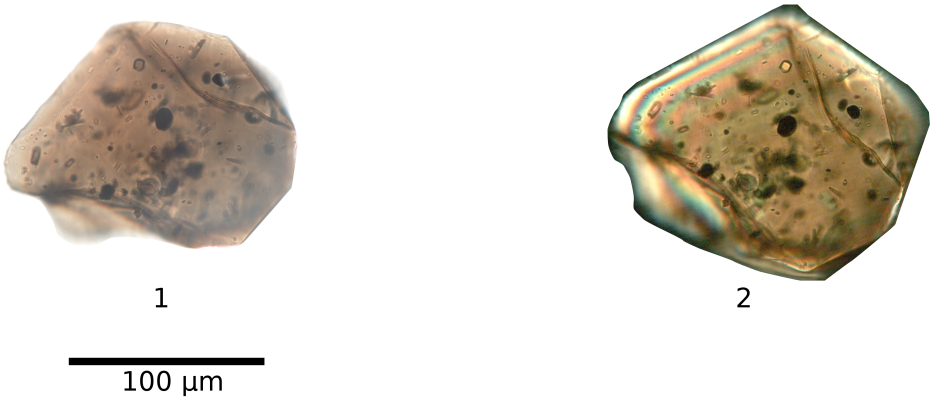

Figure A.13: Microscopy pictures of tourmaline: (1) single-polarized light, (2) crossed polarization filter

A.3.11 Zircon

Zircon has a very high relief and appears as elongated grains which show nearly no alteration marks, are less rounded and suggest to be formed in situ. The color varies between light to deep pale brown without pleochrosim. The birefringence of Zircon is very high with white in the high orders as interference color.

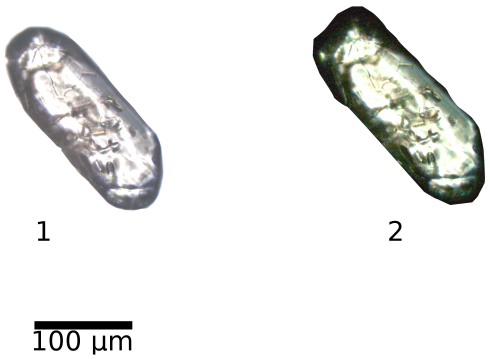

Figure A.14: Microscopy pictures of zircon: (1) single-polarized light, (2) crossed polarization filter

A.3.12 Zoisite

Zoisite appears mostly as rectangular grains with high relief and less roundness, usually fractured. Under single-polarized light it is colorless, whereas under crossed polarization filter it shows incomplete parallel extinction and abnormal interference colors of the first order. The elongation varies between the grains.

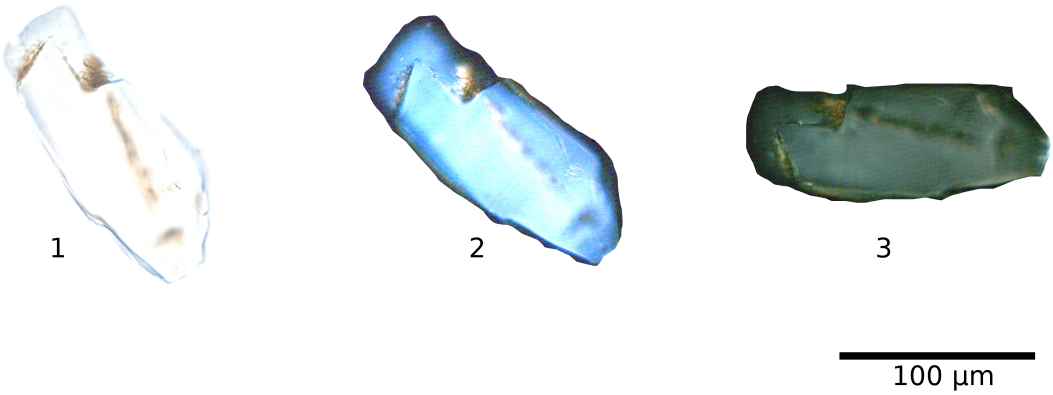

Figure A.15: Microscopy pictures of zoisite: (1) single-polarized light, (2) crossed polarization filter (maximum interference colors), (3) crossed polarization filter (incomplete extinction)

A.4 List of counting results

	MUO12-SS-01	±	MUO12-SS-02	±	MUO12-SS-03	±	MUO12-SS-04	±	MUO12-SS-05	±	MUO12-SS-06	±	MUO12-SS-07	±
Pyroxene	111	2.7	46	4.3	35	3.4	49	2.9	63	3.1	38	4.3	41	3.7
Garnet	49	1.9	34	3.8	43	3.7	49	2.9	48	2.8	22	3.4	44	3.8
Amphibol	302	3.6	109	5.7	126	5.3	205	4.7	180	4.5	118	6.1	116	5.4
Zircon	36	1.6	17	2.8	18	2.5	26	2.2	41	2.6	15	2.8	29	3.2
Epidot-Group	52	1.9	18	2.9	23	2.8	25	2.1	17	1.7	20	3.2	21	2.8
Apatite	41	1.7	22	3.2	23	2.8	28	2.3	46	2.7	10	2.3	26	3.0
Kyanite	27	1.4	10	2.2	6	1.5	17	1.8	23	2.0	9	2.2	9	1.8
Tourmaline	2	0.4	1	0.7	0	0.0	1	0.4	0	0.0	1	0.8	0	0.0
Rutile	1	0.3	0	0.0	0	0.0	0	0.0	0	0.0	0	0.0	3	1.1
Opaque minerals	77	2.3	24	3.3	50	3.9	46	2.8	41	2.6	30	3.9	26	3.0
red Aggregates	31	1.5	5	1.5	9	1.8	9	1.3	10	1.3	2	1.1	6	1.5
Sum	729		286		333		455		469		265		321	

	MUO12-SS-08	±	MUO12-SS-09	±	MUO12-SS-10	±	MUO12-SS-11	±	MUO12-SS-12	±	MUO12-SS-13	±	MUO12-SS-14	±
Pyroxene	73	2.3	25	3.5	36	4.8	35	4.2	42	3.6	48	2.8	65	3.6
Garnet	101	2.7	19	3.1	19	3.6	27	3.8	33	3.2	48	2.8	52	3.3
Amphibol	234	3.6	70	5.3	65	6.0	106	6.1	119	5.2	214	4.6	146	4.7
Zircon	51	2.0	22	3.3	20	3.7	18	3.1	34	3.3	41	2.6	25	2.4
Epidot-Group	40	1.8	20	3.2	26	4.2	22	3.4	34	3.3	33	2.4	29	2.5
Apatite	39	1.8	12	2.5	24	4.0	12	2.6	24	2.8	32	2.3	32	2.6
Kyanite	15	1.1	4	1.5	5	1.9	3	1.3	5	1.3	6	1.0	8	1.4
Tourmaline	4	0.6	0	0.0	1	0.9	4	1.5	1	0.6	0	0.0	1	0.5
Rutile	8	0.8	1	0.7	1	0.9	1	0.8	0	0.0	2	0.6	3	0.8
Opaque minerals	122	2.9	20	3.2	32	4.6	22	3.4	42	3.6	42	2.6	44	3.1
red Aggregates	3	0.5	77	5.5	0	0.0	12	2.6	5	1.3	1	0.4	5	1.1
Sum	690		270		229		262		339		467		410	

	MUO12-SS-15	±	MUO12-SS-16	±	MUO12-SS-17	±	MUO12-SS-18	±	MUO12-SS-19	±	MUO12-SS-20	±	MUO12-SS-21	±
Pyroxene	39	2.7	24	4.0	55	3.0	53	3.3	53	3.2	38	3.9	54	3.4
Garnet	50	3.0	27	4.2	58	3.0	38	2.8	51	3.2	34	3.7	60	3.5
Amphibol	201	4.7	98	6.5	216	4.6	196	4.9	194	4.9	139	5.8	139	4.7
Zircon	24	2.1	13	3.0	32	2.3	30	2.5	27	2.4	16	2.6	30	2.6
Epidot-Group	42	2.8	24	4.0	38	2.5	43	3.0	26	2.4	18	2.8	29	2.6
Apatite	13	1.6	10	2.6	23	2.0	21	2.2	21	2.1	12	2.3	21	2.2
Kyanite	8	1.3	4	1.7	8	1.2	6	1.2	4	1.0	2	1.0	2	0.7
Tourmaline	1	0.4	2	1.2	2	0.6	0	0.0	0	0.0	1	0.7	0	0.0
Rutile	2	0.6	0	0.0	1	0.4	0	0.0	0	0.0	0	0.0	1	0.5
Opaque minerals	66	3.4	31	4.4	39	2.5	27	2.4	42	2.9	28	3.4	42	3.0
red Aggregates	1	0.4	1	0.9	0	0.0	0	0.0	1	0.5	6	1.6	28	2.5
Sum	447		234		472		414		419		294		406	

	MUO12-SS-22	±	MUO12-SS-23	±	MUO12-SS-24	±
Pyroxene	41	3.2	45	3.1	33	3.0
Garnet	47	3.4	50	3.3	54	3.7
Amphibol	149	5.0	170	4.9	159	5.2
Zircon	27	2.7	26	2.4	19	2.3
Epidot-Group	35	3.0	40	3.0	39	3.3
Apatite	15	2.0	22	2.3	26	2.7
Kyanite	1	0.5	2	0.7	2	0.8
Tourmaline	0	0.0	0	0.0	0	0.0
Rutile	1	0.5	3	0.9	1	0.6
Opaque minerals	52	3.6	38	2.9	27	2.8
red Aggregates	9	1.6	9	1.5	3	1.0
Sum	377		405		363	

Figure A.16: Counting results as absolute values

	MUO12-SS-01	MUO12-SS-02	MUO12-SS-03	MUO12-SS-04	MUO12-SS-05	MUO12-SS-06	MUO12-SS-07	MUO12-SS-08
Pyroxene	15.2	16.1	10.5	10.8	13.4	14.3	12.8	10.6
Garnet	6.7	11.9	12.9	10.8	10.2	8.3	13.7	14.6
Amphibol	41.4	38.1	37.8	45.1	38.4	44.5	36.1	33.9
Zircon	4.9	5.9	5.4	5.7	8.7	5.7	9	7.4
Epidot-Group	7.1	6.3	6.9	5.5	3.6	7.5	6.5	5.8
Apatite	5.6	7.7	6.9	6.2	9.8	3.8	8.1	5.7
Kyanite	3.7	3.5	1.8	3.7	4.9	3.4	2.8	2.2
Tourmaline	0.3	0.3	0	0.2	0	0.4	0	0.6
Rutile	0.1	0	0	0	0	0	0.9	1.2
Opaque minerals	10.6	8.4	15	10.1	8.7	11.3	8.1	17.7
red Aggregates	4.3	1.7	2.7	2	2.1	0.8	1.9	0.4
Percentage Alterites of all counted grains	40.6	46.5	30.8	43.5	38.2	38.4	57.1	37.1

	MUO12-SS-09	MUO12-SS-10	MUO12-SS-11	MUO12-SS-12	MUO12-SS-13	MUO12-SS-14	MUO12-SS-15	MUO12-SS-16
Pyroxene	9.3	15.7	13.4	12.4	10.3	15.9	8.7	10.3
Garnet	7	8.3	10.3	9.7	10.3	12.7	11.2	11.5
Amphibol	25.9	28.4	40.5	35.1	45.8	35.6	45	41.9
Zircon	8.1	8.7	6.9	10	8.8	6.1	5.4	5.6
Epidot-Group	7.4	11.4	8.4	10	7.1	7.1	9.4	10.3
Apatite	4.4	10.5	4.6	7.1	6.9	7.8	2.9	4.3
Kyanite	1.5	2.2	1.1	1.5	1.3	2	1.8	1.7
Tourmaline	0	0.4	1.5	0.3	0	0.2	0.2	0.9
Rutile	0.4	0.4	0.4	0	0.4	0.7	0.4	0
Opaque minerals	7.4	14	8.4	12.4	9	10.7	14.8	13.2
red Aggregates	28.5	0	4.6	1.5	0.2	1.2	0.2	0.4
Percentage Alterites of all counted grains	47.2	55.7	55.7	51.8	42.2	40.5	37.7	52.7

	MUO12-SS-17	MUO12-SS-18	MUO12-SS-19	MUO12-SS-20	MUO12-SS-21	MUO12-SS-22	MUO12-SS-23	MUO12-SS-24
Pyroxene	11.7	12.8	12.6	12.9	13.3	10.9	11.1	9.1
Garnet	12.3	9.2	12.2	11.6	14.8	12.5	12.3	14.9
Amphibol	45.8	47.3	46.3	47.3	34.2	39.5	42	43.8
Zircon	6.8	7.2	6.4	5.4	7.4	7.2	6.4	5.2
Epidot-Group	8.1	10.4	6.2	6.1	7.1	9.3	9.9	10.7
Apatite	4.9	5.1	5	4.1	5.2	4	5.4	7.2
Kyanite	1.7	1.4	1	0.7	0.5	0.3	0.5	0.6
Tourmaline	0.4	0	0	0.3	0	0	0	0
Rutile	0.2	0	0	0	0.2	0.3	0.7	0.3
Opaque minerals	8.3	6.5	10	9.5	10.3	13.8	9.4	7.4
red Aggregates	0	0	0.2	2	6.9	2.4	2.2	0.8
Percentage Alterites of all counted grains	37.2	38.3	39.5	58.5	55.5	52.9	47.7	36.9

Figure A.17: Counting results as relative values